

**REVIEW OF AERONAUTICAL FATIGUE
INVESTIGATIONS IN JAPAN
DURING THE PERIOD JUNE 2021 TO MAY 2023**

Edited by

Takao Okada

Japan Aerospace Exploration Agency

For Presentation at the 37th Conference of
the International Committee on Aeronautical Fatigue and Structural Integrity

Delft, the Netherland, 26-29 June, 2023

CONTENTS

	page
<u>1. INTRODUCTION</u>	1
<u>2. FATIGUE AND FAILURE IN METALLIC MATERIALS AND COMPONENTS</u>	
2.1 Practical Ductile Fracture Criterion Model for Aerospace Structure Static Strength Evaluations Using Detailed FE Analysis	3
2.2 Development of methods for microtexture characterization and dwell fatigue life prediction of dual phase titanium alloys	4
2.3 Fatigue fracture mechanics of selective laser PBF titanium alloy	4
2.4 Revealing mechanisms of creep-fatigue crack propagation in Ni-base superalloys for turbine disks: Towards application of damage tolerant design and maintenance	4
2.5 Research for thermal load and procedure to predict fatigue life up to form a fatigue crack on CFRP/Aluminium hybrid joints	6
<u>3. FATIGUE AND FAILURE IN COMPOSITE MATERIALS AND COMPONENTS</u>	
3.1 Consideration of life prediction model for ceramic matrix composite(CMC) with cooling hole	7
3.2 A numerical scheme for fatigue simulation of laminated composites using CZM-XFEM and cohesive element	7
3.3 Giga-cycle fatigue properties of transverse crack initiation in cross-ply CFRP laminates using ultrasonic fatigue testing	7
3.4 Development of CFRP with improved lightening resistance using electrically conductive resin	8

3.5 DCB Test Automated with Crackgages	9
--	---

4. NDI

4.1 A wavelet analysis method for defects detection in CFRP composites with fully non-contact lamb waves	10
--	----

5. MISCELLANEOUS

5.1 High-degree-of-freedom composite technology using thin-layer materials that exploit the potential of composite materials	11
5.2 Optimal design and static load testing of tow-steered aircraft fuselage frames	12
5.3 Clarifying Edge Glow Mechanisms of CFRP Exposed to Simulated Lightning Current in In-Plane Direction	12
5.4 Aircraft Accident and Serious Incident Investigation	13

<u>ACKNOWLEDGEMENTS</u>	15
--------------------------------	----

<u>TABLES AND FIGURES</u>	16
----------------------------------	----

1. INTRODUCTION

Takao Okada, Japan Aerospace Exploration Agency

This review summarizes the papers on the study of aeronautical fatigue, structural integrity and related themes conducted in Japan during June 2021 to May 2023.

The papers were contributed by following organizations:

IHI Corporations

Japan Aerospace Exploration Agency (JAXA)

Japan Transport Safety Board (JTSB)

Kawasaki Heavy Industries, Ltd. (KHI)

Kiguchi Technics inc.

Mitsubishi Heavy Industries, Ltd. (MHI)

Shoden Corporation

SUBARU CORPORATION

Tokyo University of Agriculture and Technology

The University of Tokyo

Waseda University

Yamagata University

The general activities on aircraft development program in Japan during 2021 to 2023 is summarized as follows:

- JAXA establishes the consortium named Comprehensive Aviation Innovation by digital transformation (CHAIN-X) at June 17 in 2022, in order to increase an aviation industry in Japan, enhance its international competitiveness and develop a human resource work at digital transformation (DX) in aviation industry. Ministry of economy, trade and industry and 11 related organizations participate in CHAIN-X. CHAIN-X acts as central role for research and development in the field of optimization and acceleration using DX in design, certification, manufacturing, operation and recycle of aircraft.
- Ministry of land, infrastructure and transport and Ministry of economy, trade and industry jointly organize a council to discuss emerging technology for de-carbonization in aviation. Public and Private sector are involved in the council and working group for motorization, hydrogen powered and weight reduction are established.
- Second phase of SIP (Cross-ministerial Strategic Innovation Promotion Program) supported by

the Council for Science, Technology and Innovation (CSTI) of the Cabinet Office, Japan have been conducted between 2018 and 2022. From the material development point of view, its purpose is to develop a next-generation Materials Integration (MI) system for the inverse design creating desired performance, materials and process, leading the world utilizing the technical foundation of MI being developed so far. Following three domains construct the research project: A: Establishment of Inverse Design MI Basis for Advanced Structural Materials and Processes, B: Application of the Inverse Design MI to Actual Structural Materials (CFRP), and C: Application of the Inverse Design MI to Actual Structural Materials (3D Powder Processing). The developed material and process plan to use the aircraft structure and the engine.

- The WEATHER (Weather Endurance Aircraft Technology to Hold, Evade and Recover) -Eye consortium is established in 2016, in order to improve the operational safety and efficiency under the severe weather condition such as slippery short runway, severe lightning, crystal ice drop and volcanic ash. From the material point of view, development of the CFRP with high conductivity through the thickness direction using conductive polymer have been conducted to reduce the lightning damage. High conductive polymer using polyaniline (PANI) is developed and the reduction of the lightning damage using the polymer is demonstrated. The modification of the polymer is underway.

The copyright at section 3.4, 3.5 and 5.3 belongs to The Japan Society of Aeronautical and Space Sciences (JSASS).

2 FATIGUE AND FAILURE IN METALLIC MATERIALS AND COMPONENTS

2.1 Practical Ductile Fracture Criterion Model for Aerospace Structure Static Strength Evaluations Using Detailed FE Analysis

Takuya Ishida¹, Tsutomu Yoshida¹

¹Kawasaki Heavy Industries, Ltd., Kakamigahara, Japan

The application of detailed FE analysis can contribute to structural evaluations for all kinds of aerospace structure, without any simplification to some “Handbook” models by engineering judgments. However, it’s difficult to evaluate the static strength quantitatively on detailed FE analysis, due to a lack of the sound and practical ductile fracture criterion. Kawasaki Heavy Industries, Ltd. (KHI) has developed a practical ductile fracture criterion for the detailed FE analysis, which can consider the stress triaxiality and the strength anisotropy [1].

Some casual engineers might evaluate the static strength of metallic structures by comparing the von Mises equivalent stress obtained from the FE analysis against the tensile ultimate stress design allowable (Ftu). This simple approach might be convenient, but the actual ductile fracture behavior of the metallic materials is highly dependent of the stress triaxiality[2] (Fig.2.1.1). Thus, KHI has focused on the Coulomb-Mohr criterion (C-M criterion), that is a widely-used fracture criterion in the field of geotechnical engineering such as rock mechanics, because the C-M criterion deals the stress triaxiality as an essential variable to estimate the material mechanical behavior.

A series of static strength coupon tests are performed for the common aerospace metallic materials, AL7050-T7451, AL2124-T851, Ti-6AL-4V. And, the internal stress distributions at the instance of test specimen fractures are estimated using the detailed non-linear FE analysis of these test specimens. As a result of these efforts, we confirmed that there is an apparent trend of the maximum shear stress upper bounds being a linear function of hydrostatic stress (Fig.2.1.2). This trend implies that the C-M criterion can be applied to the ductile fracture of these metallic materials, as suggested from the pioneering work by Bai [3].

Another point to emphasize is that the metallic materials used in the aerospace industry exhibit strength anisotropy. As the C-M criterion is an isotropic criterion, it cannot express any strength anisotropy by itself. It is possible to use the minimum property regardless of the grain directions. However, this approach might lead to over-conservatism.

KHI took the approach of linear transformations, from the actual working stress domain to anisotropy-converged stress domain, to express the strength anisotropies (Fig.2.1.3). This proposed anisotropic extension schema for the C-M criterion (TCM: Transformed Coulomb-Mohr model) is as follow.

$$\begin{bmatrix} \sigma'_{11} \\ \sigma'_{22} \\ \sigma'_{33} \\ \sigma'_{12} \\ \sigma'_{13} \\ \sigma'_{23} \end{bmatrix} = T_{TCM} \begin{bmatrix} \sigma_{11} \\ \sigma_{22} \\ \sigma_{33} \\ |\sigma_{12}| \\ |\sigma_{13}| \\ |\sigma_{23}| \end{bmatrix}, \quad T_{TCM} = \begin{bmatrix} A & B & C & F & G & H \\ B & A & C & F & H & G \\ D & D & E & I & J & J \\ K & K & L & P & & \\ M & N & O & & Q & \\ N & M & O & & & Q \end{bmatrix} \quad (\text{linear transformation})$$

$$f(\sigma'_{11}, \sigma'_{22}, \sigma'_{33}, \sigma'_{12}, \sigma'_{13}, \sigma'_{23}, m'_{TCM}) = \tau_{uTCM} \quad (\text{TCM criterion})$$

where subscripts 1, 2, 3 denote material grain directions L, LT, and ST respectively. T_{TCM} is linear transformation matrix, and each term of the matrix is obtained using any numerical optimization technic. m'_{TCM} and τ_{uTCM} are material constants.

To make a practical implementation of the TCM model, KHI has developed the method to create the above material properties, using some well-established statistically based metallic material allowable data, such as MMPDS[4]. And KHI has developed an in-house user subroutine, in order to easily apply the TCM material model under the nonlinear static analysis.

To demonstrate the predictive capability of the TCM model, a diagonal tension beam test result (Fig.2.1.4) and the accompanying nonlinear static analyses is presented. The FE model with the TCM material model based on the A-basis design allowable from MMPDS

are prepared. Fig.2.1.5 shows the FE analysis results predicting the ductile fracture of the test specimen. The TCM model predicts the fracture due to biaxial tension at $0.95 P_{TEST}$ along the ridge of the convex wrinkle. Further more detail of this demonstration and other verification results are reported in reference [1].

It is demonstrated that the TCM model has the superior predictive capability for ductile fracture phenomenon. The use of TCM model will make it possible to design the innovative structural configurations previously very difficult to explore.

References

- [1] Yoshida, Tsutomu and Ishida, Takuya, "Practical Ductile Fracture Criterion Model for Metallic Aerospace Structure Static Strength Evaluations," Proceedings of the ASME 2023 Aerospace Structures, Structural Dynamics, and Materials Conference, June 19-21, 2023, San Diego, California
- [2] Bao, Yingbin and Wierzbicki, Tomasz, "On Fracture Locus in the Equivalent Strain and Stress Triaxiality Space," International Journal of Mechanical Sciences Vol.46 No.1 (2004): pp.81-98
- [3] Bai, Yuanli and Wierzbicki, Tomasz, "Application of extended Mohr–Coulomb criterion to ductile fracture," International Journal of Fracture Vol.161 No.1 (2010): pp.1-20
- [4] "Metallic Materials Properties Development and Standardization (MMPDS)," Technical Report No. MMPDS-16. Battelle Memorial Institute, Columbus, OH. 2021.

2.2 Development of Methods for Microtexture Characterization and Dwell Fatigue Life Prediction of Dual Phase Titanium Alloys

Masayuki Tsukada¹, Koichi Inagaki¹, Itsuki Kawata¹, Shigeru Yasuda², Toko Hamaguchi², Yoshihiro Otani², Yuta Kitamura², Shinya Miyazaki²

¹ Aero engine space & Defense business area, IHI Co., Ltd

² Technology & Intelligence Integration, IHI Co., Ltd

Near alpha and alpha plus beta titanium alloy can exhibit large reductions of dwell fatigue life. These reductions result from the formation of commonly oriented microscopic α -phase regions called microtexture (MTR). In this study, electron backscatter diffraction (EBSD), spatially resolved acoustic spectroscopy (SRAS) and ultrasonic testing have been used for characterization of MTR. The results of in-situ dwell fatigue test by digital image correlation (DIC) and the related quantitative fractography have been utilized to establish the role of MTR for dwell fatigue fracture (Figure 2.2.1). To develop a physical model to predict dwell fatigue life reduction depending on MTR, crystal plasticity analysis also has been conducted (Figure 2.2.2). This recently acquired information aims to be used to create a tool to estimate reduction of dwell fatigue life by non-destructive ultrasonic evaluation of titanium forgings, which will enable classification of materials from a MTR perspective and will support improvement of material quality in actual production. Results for Ti-64 will be presented here as it is a widely used alloy.

2.3 Fatigue fracture mechanics of selective laser PBF titanium alloy

Akiko Kasami¹, Shinya Suzukake¹, Sayaka Maruta¹, Yuta Imai¹, Hiroshi Ishikawa¹

¹ Mitsubishi Heavy Industries

The strength properties of AM materials are greatly changed by defects and microstructure. Especially, titanium alloy is easy to change surface and internal defect and microstructure by the difference of quality of the powder, molding equipment, molding parameter, type of heat treatment, and the mechanical property greatly changes by it. Therefore, the purpose of this study was to clarify experimentally the effects of defects and microstructure on the strength properties of AM titanium alloy formed by laser Powder Bed Fusion. The microstructure and internal and/or surface defects of additive manufactured titanium alloy Ti-6Al-4V are highly rely on the post heat treatment conditions including HIP and they have a strong relationship with fatigue properties. The relationship between internal defects and microstructure and role of defects in additive manufactured Ti-6Al-4V was evaluated by fatigue test and also detailed investigation based on fracture mechanics were conducted (Figure 2.3.1).

2.4 Revealing Mechanisms of Creep-Fatigue Crack Propagation in Ni-base Superalloys for Turbine Disks: Towards Application of Damage Tolerant Design and Maintenance

Shiyu Suzuki^{1,2}, Hayato Matsuoka², Zhang Qihe², Otsuka Sasakura², Motoki Sakaguchi²

¹ Japan Aerospace Exploration Agency (JAXA), Tokyo, Japan

² Tokyo Institute of Technology, Tokyo, Japan

Ni-base superalloys are widely used for turbine disks in jet engines. During services of the engines, the superalloys are subjected to creep-fatigue loading due to repeated turbine start-up and shut-down as well as steady-state operations. The classical safe-life approach requires replacements of all components at a pre-defined cycle, which may result in unnecessary retirements of components that are still able to be used in the service. To reduce costs for the replacements, the damage tolerant approach is desired to be applied to the design and maintenance of the turbine disks. The damage tolerant approach consists of non-distractive inspection of cracks and prediction of their propagation. The latter is especially difficult since the crack propagation under the creep-fatigue loading (creep-fatigue crack propagation) is a complex phenomenon due to an interaction between effects of creep, fatigue and environment. In particular, the effect of creep loading on the crack propagation during subsequent fatigue loading has not been fully understood. This study aims to reveal fundamental mechanism of the effect of creep loading on the subsequent fatigue crack propagation by means of crack propagation tests and numerical simulations, and to contribute to more accurate prediction of the creep-fatigue crack propagation. The schematic of this study is shown in Fig. 2.4.1.

Compact tension (C(T)) specimens with 1 mm thickness were manufactured from a wrought Ni-base superalloy, Inconel 718, which is a typical disk material. The material was produced as in compliant with AMS5663 standard, and a grain size was about 30 μm . The crack propagation tests were conducted at 650 $^{\circ}\text{C}$. To isolate the effect of creep loading, the crack propagation tests were conducted by applying single tension hold during pure fatigue loading. More specifically, loading sequences consisted of three parts:

- (1) Pure fatigue loading under $\Delta K = 10, 12$ or $15 \text{ MPam}^{1/2}$ constant condition with a load ratio of 0.4 and a frequency of 10 Hz.
- (2) Tension hold at K_{max} values of the load sequence (1), which are 16.7, 20 or $25 \text{ MPam}^{1/2}$, respectively. Hold time was 45, 90 or 180 minutes. When the K_{max} values were 20 or $25 \text{ MPam}^{1/2}$, static crack propagation occurred during this sequence.
- (3) Pure fatigue loading under ΔK increasing condition from ΔK values of the load sequence (1).

Crack length was monitored by the potential drop method.

In the tests with initial ΔK values during the load sequence (1) of 12 or $15 \text{ MPam}^{1/2}$, the fatigue crack propagation rates were accelerated when the load sequence (3) was started after the tension hold during the sequence (2) as shown in Fig. 2.4.1(a). Scanning electron microscopy analysis on fracture surfaces revealed that the crack acceleration occurred along grain boundaries. Also, energy dispersive X-ray spectroscopy analysis on the fracture surfaces revealed high concentrations of oxygen element over areas of the crack propagation during the tension hold in the load sequence (2) and the subsequent acceleration during the load sequence (3). Thus, the crack propagation during these periods were attributed to the stress-assisted oxygen diffusion along grain boundaries and the resultant embrittlement of the grain boundaries during the tension hold. A summation of the distance of the crack propagation during the tension hold and the distance where the acceleration continued is called “thermally affected zone (TAZ) size” and plotted as a function of the K in Fig. 2.4.1(d). The TAZ size increased with the K .

In the tests with initial ΔK values during the load sequence (1) of $10 \text{ MPam}^{1/2}$, the fatigue crack propagation rates were temporarily accelerated over short distances after the tension hold during the load sequence (2) as shown in Fig. 2.4.1(b). However, it was followed by significant reduction in the fatigue crack propagation rates, which is called “crack retardation”. A similar retardation behavior was reported by the present authors [1, 2], and it was found that the retardation is caused by compressive residual stress field induced by creep deformation during the tension hold (Fig. 2.4.1(c)). In this study, the transition from the retardation to the acceleration depending on the K value is rationalized based on a simple comparison between sizes of the compressive residual stress field and the TAZ. The compressive residual stress field was calculated by finite element analysis which considered elastic, plastic and creep deformation. The results are shown in Fig. 2.4.1(d) along with the TAZ, which shows that the compressive residual stress field is larger than the TAZ when K is smaller than $18 \text{ MPam}^{1/2}$. This result explains the transition behavior.

In summary, this study investigated the effect of creep loading on the subsequent fatigue crack propagation with the aim of clarifying the mechanism of the creep-fatigue crack propagation in Ni-base superalloys. The crack propagation tests were conducted by applying single tension hold during pure fatigue loading. Both fatigue crack retardation and acceleration occurred after the tension hold depending on the K value. The transition from the retardation to the acceleration was rationalized based on a simple comparison between sizes of the compressive residual stress field and the TAZ. A research to quantitatively predict crack propagation rates during both retardation and acceleration under arbitrary load conditions is

currently being conducted by the authors to realize the damage tolerant design and maintenance of the turbine disks.

References

- [1] Shiyu Suzuki, Motoki Sakaguchi, Fatigue crack retardation associated with creep deformation induced by a tension hold in a single crystal Ni-base superalloy, *Scripta Materialia*, Vol. 178, pp. 346-350, 2020.
- [2] Shiyu Suzuki, Motoki Sakaguchi, Ryota Okamoto, Hideaki Kaneko, Takanori Karato, Kenta Suzuki and Masakazu Okazaki, Competing Mechanism of Creep Damage and Stress Relaxation in Creep-Fatigue Crack Propagation in Ni-Base Superalloys. In: , et al. *Superalloys 2020. The Minerals, Metals & Materials Series*. Springer, Cham.

2.5 Research for thermal load and procedure to predict fatigue life up to form a fatigue crack on CFRP/Aluminum alloy hybrid joints

Takao Okada¹, Hisashi Kumazawa¹, Takafumi Toyosawa¹, Tomo Takeda¹, Toshiyuki Kasahara¹, Koichi Yamada¹, Kasumi Nagao¹, Yuichiro Aoki¹ and Hirokazu Shoji¹

¹ Japan Aerospace Exploration Agency (JAXA), Tokyo, Japan

In ICAF2015, JAXA (Japan Aerospace Exploration Agency) and NRC (National Research Council) presented the life distribution up to first linkup of adjacent fatigue cracks formed in the riveted Aluminum lap joint under constant amplitude fatigue load. The fatigue life up to 0.5mm crack formation was predicted by SWT (Smith-Watson-Topper) equation and the life up to first linkup was predicted using in house code.

Currently, JAXA have been conducted the research to evaluate the fatigue life up to form a fatigue crack in a metal/composite hybrid joint. Thermal stress at high and low temperature is occurred in metal/composite hybrid joints due to the difference of coefficient of thermal expansion between metal and composite materials. For application of SWT equation to predict the fatigue life of the metal/composite hybrid joints, accurate calculation of stress and strain in the joint including thermal effect is very important. In this study, thermal load in a mechanically fastened hybrid joint under temperature cycle was investigated experimentally and numerically. In addition, material constants of aluminum sheets were obtained with the strain-controlled fatigue tests for precise prediction by SWT equation.

For the investigation of the thermal load in the hybrid joint, the mechanically fastened hybrid joint specimens composed of two aluminum plates and a composite plate were prepared (Figure 2.5.1). Experimental results indicated that relationships between temperature and elastic strain on specimen surface in temperature cycle exhibit hysteresis loop (Figure 2.5.2). Finite element analysis for the hybrid joint (Figure 2.5.3) was also conducted and captured the hysteresis loop obtained by the experiment.

In the material data measurements, the fatigue life for the aluminum alloy in relation to the product of the strain amplitude and the maximum stress has been obtained by the strain-controlled fatigue tests. The strain-controlled fatigue tests are terminated when applied load is reduced by the fatigue crack. The obtained cycles are planned to evaluate the life for formation of certain crack size represented by the applied load reduction to 95% of the maximum load, and the relationship between the crack formation cycles and the product of the maximum stress and the strain amplitude are obtained (Figure 2.5.4). The obtained relationship would be used to preliminary predict a fatigue crack formation life of the hybrid joint using FEM result.

3. FATIGUE AND FAILURE IN COMPOSITE MATERIALS AND COMPONENT

3.1 Consideration of Life Prediction Model for Ceramic Matrix Composite (CMC) with Cooling Hole Hayao Sato¹, Daichi Haruyama¹, Hiroshi Nakamura¹, Tatsuhito Honda¹, Masahiro Hojo²

¹ Aero engine space & Defense business area, IHI Co., Ltd

² Japan Aerospace Exploration Agency (JAXA)

Ceramic matrix composites (CMCs) have higher heat resistance and specific elasticity than Ni-based alloys, thus it is desired to be applied to aircraft engines such as turbine parts. In high temperature parts, small holes should be pierced to inject cold fluid (Figure 3.1.1). However, there are few research on the effect of small hole against the CMC fatigue life. This study focused to this phenomenon. Fatigue tests were conducted using flat plates pierced with single hole and multiple holes. Multiple holes were allocated vertically against load direction. Multiple holes have more advanced hole shapes which is called diffuser hole.

In the test results, different fracture mode and crack propagation were observed between single holed and multiple holed type. Multiple holed specimens had shorter lives than single hole. In addition, the fatigue lives of diffuser hole were shorter than circular hole.

For evaluating life shorting of multiple holed specimens, life prediction models were reconsidered, which includes stress prediction and life prediction. The strength parameters were calculated by averaging stress field, which were predicted by finite element analysis (FEA), in area of CMC unit cell (Figure 3.1.2). After evaluating lives of hole specimens, multiple holed lives were predicted by using a smooth test S-N curve. Furthermore, to improve the stress prediction, the strength parameters were recalculated after resizing diffuser hole shape to fit the actual specimen. After that, all specimen lives were predicted around smooth specimen's S-N curve regardless of the number of holes. Finally, we have established the life prediction model for the holed CMCs.

Acknowledgement

The work presented in this paper is based on research conducted in En-Core project. The authors would like to thank all persons and organizations involved in this work for their supports.

3.2 A Numerical Scheme for Fatigue Simulation of Laminated Composites using CZM-XFEM and Cohesive Element

Rong-Can Hong¹, Ryo Higuchi¹ and Tomohiro Yokozeki¹

¹ The university of Tokyo, Tokyo, Japan

A numerical method for fatigue damage accumulation in laminated composites is developed in this paper. Extended finite element method (XFEM) and cohesive element are integrated into a numerical program for fatigue fracture. In this work, XFEM and cohesive element are applied for modelling matrix cracking and delamination in CFRP laminates respectively. A fatigue model based on cohesive zone model (CZM) is also introduced into the numerical scheme. Standard DCB and ENF fatigue tests are used as the identification of parameters of the fatigue model, and simulation models of the standard tests are established for calibrating the fatigue model of pure mode. With the parameters calibrated by the benchmarks of pure mode tests, the numerical analysis of open hole tensile (OHT) test is conducted to investigate the fracture behaviours of composite laminates under cyclic loading. The delamination, splitting in the 0° plies and transverse cracking in the 90° plies are all predicted in the numerical results. The progression of fatigue damage in the simulation model is consistent with previous experimental work. This study demonstrates that the proposed numerical method can correctly predict the initiation and evolution of fatigue damage under mixed mode loading. By XFEM, in-ply matrix cracking can be modelled as multiple mesh-independent path in FE model. This paper provides a convenient approach utilizing the features of XFEM for simulating fatigue cracking in composite laminates.

3.3 Giga-Cycle Fatigue Properties of Transverse Crack Initiation in Cross-ply CFRP Laminates using Ultrasonic Fatigue Testing

Atsushi Hosoi*, Shinji Ito, Tsuyoshi Miyakoshi, Shima Momoka, Yuki Nishi, Hikaru Saito and Hiroyuki Kawada

* Waseda University, Tokyo, Japan

An application of carbon fiber reinforced plastic (CFRP) laminates is being expanded to rotating components such as jet engine fan blades. Since the blade members are subjected to cyclic loading exceeding 10^9 cycles during their design life, it is important to clarify the gigacycle fatigue properties of CFRP laminates and their fracture mechanisms. Thus, the objective of this study was to evaluate the gigacycle fatigue properties of CFRP laminates in transverse crack initiation. A conventional hydraulic fatigue test is too time-consuming, and accelerated tests must be conducted to evaluate gigacycle fatigue properties. In this study, accelerated fatigue tests were conducted at a test frequency of 20 kHz by ultrasonic fatigue testing as shown in Fig. 3.3.1. The temperature rise of the specimens due to self-heating was prevented by air cooling with dry air and intermittent operation. Therefore, the apparent test frequency was approximately 1.8 kHz. So far, no definite fatigue limit of CFRP laminates has been confirmed. It is known that the initial damage in fatigue of CFRP laminates is transverse cracks, and that its growth and increase can lead to major damage such as delamination and fiber breakage. It is possible to obtain the initial fatigue properties before macroscopic damage occurs by evaluating the initiation life of transverse cracks. In addition, a mechanical model based on a variational approach was proposed for a cross-ply laminates with transverse cracks resonated in the first-order mode by ultrasonic vibration. In this study, $[0/90_6]_s$ cross-ply CFRP laminates were used, and the fatigue test was conducted at a stress ratio of $R = -1$ by the hydraulic fatigue and the ultrasonic fatigue testing. The experimental results showed that no transverse crack initiation occurred in the giga-cycle region, suggesting the existence of the fatigue limit as shown in Fig. 3.3.2. The stress analysis results of the proposed model showed good agreement with the results of the finite element analysis.

3.4 Development of CFRP with improved lightning resistance using electrically conductive resin Tomohiro Yokozeki¹, Teruya Goto², Tatsuhiro Takahashi², Takao Okada³, Hiromitsu Miyaki³ and Shintaro Kamiyama³

¹The university of Tokyo, Tokyo, Japan

²Yamagata university, Yamagata, Japan

³Japan Aerospace Exploration Agency, Tokyo, Japan

Japanese operators encounter about 100 lightning strikes on aircraft each year, although the number can vary greatly between years, and these are often caused by cumulonimbus in the summer and by winter lightning over the Japan Sea in the winter. Winter lightning is a phenomenon observed only around the Japan Sea, the Atlantic coast of Norway, the Great Lakes and the British Isles. Cloud associated with winter lightning forms at around 500 m altitude at any time of day or night, while that concerning to cumulonimbus locates at higher altitude. The electrical discharge of winter lightning is about a hundred times greater than that of the lightning associated with cumulonimbus.

Composite materials have low electrical conductivity compared to conventional metal structures and therefore greater damage is caused in case the lightning attaches to the aircraft structure using composite material. The damage mechanism of the CFRP under lightning is much complicated and there has been much research into the lightning resistance of composite materials [1-3]. It is well known that the low electrical conductivity of the epoxy resin affects to the electrical conductivity of CFRP. To overcome this disadvantage, we improve the electrical conductivity of the resin using electrically conductive polyaniline (PANI) thermally doped by the dodecyl benzene sulfonic acid (DBSA). The developed thermoset resin consists of PANI, DBSA and divinylbenzene (DVB) as crosslinking polymer. Through the thickness electrical conductivity of CFRP using electrically conductive resin is 0.93 S/cm, while the conventional CFRP prepared for comparison is 0.06 S/cm in this research. The lightning resistance of the developed CFRP is evaluated by the simulated lightning test based on the SAE ARP-5412 with peak current reduced to -40kA and -100kA. Figure 1 shows the setup of the lightning test and figure 2 shows the NDI results for -40kA. It is confirmed that lightning damage for developed CFRP is apparently suppressed comparing to that for conventional one.

One of the drawback of PANI-based CFRP is the cationic polymerization of monomers at room temperature when the PANI/DBSA is mixed with the DVB. It rapidly increases viscosity of the resin and decreases the formability of the CFRP. In recent years, we have been working to improve this drawback by adding the extra polymer to prevent curing reaction at room temperature.

References

- [1] Y. Hirano, S. Katsumata, Y. Iwahori, A. Todoroki, "Artificial lightning testing on graphite/epoxy composite laminate", *Composites Part A*, **41**, pp. 1461-1470, (2010).
- [2] T. Ogasawara, Y. Hirano, A. Yoshimura, "Coupled thermal-electrical analysis for carbon fiber/epoxy

- composites exposed to simulated lightning current”, *Composites Part A*, **41**, pp. 973-981, (2010).
- [3] P. Feraboli, D. Miller, “Damage resistance and tolerance of carbon/epoxy composite coupons subjected to simulated lightning strike”, *Compos. Part A* 40, pp. 954-967, (2009)

3.5 DCB Test Automated with Crackgages

Eiichi Hara¹, Takashi Yamazaki², Hisaya Katoh¹ and Tetsuya Morimoto¹

¹ Japan Aerospace Exploration Agency, Tokyo, Japan

² Kiguchi Technics inc., Shimane, Japan

Double Cantilever Beam (DCB) test method requires to control cross head depending on the crack length and to measure the crack length on both side of the specimen. Therefore, test operator must continue observing specimen and controlling test machine for several hours. It is quit time and cost consuming and requires amount of period to collect test data. Although the calculation of crack length using compliance method is proposed in ref. 1, the procedure does not measure the crack length on both side of the specimen described in the standard. JAXA proposes the automating DCB test procedure using the crackgage to measure the crack length. The crackgages are attached on both side of the specimen by an adhesive and the crack length is measured as an elastic signal. The signal is used to control cross head of test machine.

Unidirectional prepreg Toray T800S/3900-2B is used to prepare the specimen. The stacking sequence is [0]¹⁴ and an insert film with 12.5mm thick is located between 7th and 8th layer to introduce the initial crack. Figure 3.5.1 shows the DCB test specimen and test fixture with 70mm crackgage, made by Kyowa Electric Instruments Co. Ltd. Followings are the DCB test procedure and the sequence between 2 and 6 are automated in this report.

1. Test start (cross head moves toward loading direction)
2. Cross head moves toward unloading direction, in case the crack length reaches the planned length.
3. Cross head moves toward loading direction, in case the load decreases to the planned value.
4. Sequence 2 and 3 are repeated until the crack length reaches the planned maximum length.
5. Cross head moves toward unloading direction.
6. Cross head stops and test is terminated.

Figure 3.5.2 shows the R-Curve obtained by the automated DCB tests. The obtained interlaminar fracture toughness described as solid and dashed line in the figure are close to that obtained by the conventional procedure [2]. Table 1 shows the procedure for conventional and proposed DCB test and the time required. The table indicates that the total time for proposed procedure becomes about one fourth of that for the conventional one, although procedure using crackgages requires the time for preparation. This procedure also can be used for DCB test in chamber as well, because the proposed procedure measures the crack length without visual inspection.

Reference

- [1] K. Kageyama, et. al., Mode I Interlaminar Fracture Mechanics of Unidirectionally Reinforced Carbon/Epoxy Laminates, *Transaction of JSME (in Japanese)*, No. 53, Vol. 494, 1987, pp. 1898-1904.
- [2] T. Morimoto, et. al., JAXA Advanced Composites Database, JAXA Research and Development Memorandum, JAXA-RM-14-004, March 2015.

4 NON DESTRUCTIVE INSPECTION

4.1 A Wavelet Analysis Method for Defects Detection in CFRP Composites with Fully Non-Contact Lamb Waves Propagation

Lea A.C. Lecointre*, Ryo Higuchi, Tomohiro Yokozeki, Shota Tonegawa, Masakatsu Mita, Naoki Hosoya and Shin-ichi Takeda

¹ The university of Tokyo, Tokyo, Japan

Ultrasonic Testing (UT) is the most common Non-Destructive Testing method used for Composite materials. One of the most promising methods which have been identified in the recent years in order to improve the efficiency of UT is the Lamb Waves Testing. However, Lamb Waves propagation is a complex phenomenon which requires adapted and efficient Signal Processing method.

In this study, we propose a method based on the Wavelet Analysis to process experimental Lamb Wave signals propagated into Carbon Fibers Reinforced Plastics (CFRP) samples for detecting artificial defects. Moreover, this experiment uses fully non-contact generation and reception of the Lamb Waves which shows very promising applications for maintenance or complex geometries.

The Lamb Waves were generated in several healthy and artificially delaminated CFRP test samples from a Laser Induced Plasma system. The reception of the propagating waves was performed by measurement of the out-of-plane displacement with a Scanning Laser Doppler Vibrometer.

Then a continuous Wavelet Transform was performed on the measured signals, which allowed to store values of Wavelet Transform coefficients (cwt) in a 3D matrix in spatial, time and frequency domains. From this matrix, spatial-time analysis was performed by extraction of 2D images at each frequency sample. The experimental group velocity dispersion curves were calculated and compared with theoretical values. The results shown that the experimental group velocities had a good correlation with theory. Moreover, for 16-ply samples including delamination at the middle depth, group tend to reach the value of 8-ply structure.

Finally, a spatial-frequency analysis was performed from the 3D cwt data. Several time samples were extracted for healthy and delaminated plates. The spatial-frequency data for healthy samples were used as baseline for detecting signals in samples containing delamination. The results shown clear and accurate localization of wide delamination from the visible increase of cwt amplitude and frequency bandwidth at the delamination zone. The same process has been performed on samples containing several small delamination. The smaller delamination ($\varnothing 10$ -mm) could not be detected, while $\varnothing 30$ - and $\varnothing 50$ -mm delamination could be detected as groups of defects.

5. MISCELLANEOUS

5.1 High-Degree-of-Freedom Composite Technology using Thin-Layer Materials that Exploit the Potential of Composite Materials

Daichi Terayama¹, Miho Yamanaka¹

¹SUBARU, Tokyo, Japan

Current composite materials are not able to demonstrate their true performance due to design constraints such as continuous stacking in the same direction and stacking order, manufacturing constraints such as using materials of a predetermined thickness, and constraints related to both design and manufacturing that are limited to combinations of linear stacking and so on. The objective of this research is to develop a high degree of freedom composite technology that removes these restrictions, increases the degree of freedom in design and manufacturing, and further brings out the characteristics of composite materials. The schematic of this study is shown in Fig. 5.1.1.

In the development of 3D high-degree-of-freedom design technology for CFRP using automated thin-layer material lamination, research and development has been conducted in three main areas: material technology, manufacturing technology, and design and analysis technology.

The material technology uses thin-layer materials that are thinner than conventional materials. Thin-layer materials allow a greater number of layers than conventional-thickness materials, which not only increases the flexibility of the lamination configuration, but also contributes to the suppression of transverse cracking, which is considered to be the starting point of fracture, and allows for higher strength than conventional-thickness laminated materials. On the other hand, thin-layer materials are more expensive due to the increase in the material manufacturing process and the increase in secondary materials, but we are conducting research and development to create low-cost materials by using a thin-layer material manufacturing process that integrates the resin impregnation process at a higher speed than before.

In manufacturing technology, we are developing the world's first technology for variable width steering lamination. In recent years, the development of automated laminating equipment has expanded the range of shapes that can be stacked, but some shapes inevitably have overlaps or gaps, and continuous fibers must be cut once. In order to address these issues, we are developing a high degree-of-freedom AFP that allows the width of the tape and lamination to be varied while steering lamination is performed.

In the area of design and analysis technology, the CoSMIC (Comprehensive System for Materials Integration of CFRP) developed in the second phase of the SIP is used to predict material strength, thereby reducing the amount of material testing, shortening design time, and reducing costs, while validating the process of building a database that can serve as the foundation for composite material design, which in the past required tolerance setting based on an extremely large number of material tests. The process of building a database is being verified. In addition, since the high degree of design freedom requires advanced design technology, which significantly increases design time and cost, research and development of optimization analysis technology that can determine the lamination configuration directly from the internal loads in the analysis is underway.

As a result, the following results were obtained.

- In material technology, we developed and introduced a one-step manufacturing line for thin-layer prepreg sheets, which enables production at a speed equivalent to that of ordinary prepreg.
- In the manufacturing technology, SUBARU succeeded in changing the width of the laminate while steering for the first time in the world. SUBARU has also demonstrated the feasibility of manufacturing actual structural parts by manufacturing a prototype propeller for use in an aircraft. The propeller made with thin-layer material and variable-width steering was approximately 18% lighter than a propeller made with conventional thick-layer material.
- In the design analysis technology, composite strength prediction was achieved through highly accurate multi-scale analysis using CoSMIC. A carpet chart was also created for use in structural design, which was used to derive the lamination configuration directly from the internal loads. Furthermore, from the optimized lamination configuration, variable width steering lamination was also optimized and the optimal lamination path was successfully output.

In the future, we will utilize the results of this research to apply the technology to air mobility and even next-generation passenger aircraft.

This work was supported by Council for Science, Technology and Innovation (CSTI), Cross-ministerial Strategic Innovation Promotion Program (SIP), “‘Materials Integration’ for Revolutionary Design System of Structural Materials” (Funding agency: JST).

5.2 Optimal Design and Static Load Testing of Tow-Steered Aircraft Fuselage Frames

Hitoshi Arizono¹, Yuichiro Aoki¹, Sunao Sugimoto¹, Ryosuke Yoshimura², Yuji Ikeda², Daisuke Nishida² and Hiroharu Suzuki²

¹ Japan Aerospace Exploration Agency, Tokyo, Japan

² Kawasaki Heavy Industries, Ltd., Kakamigahara, Japan

Weight reduction is required as one of the measures to improve the fuel consumption rate of newly developed airframes but securing the strength of high-stress areas is an issue. One of the objectives of this research is to establish a design method that secures strength by a new method that achieves fiber orientation optimization and part thickness distribution optimization at the same time. In addition, as another purpose, it is shown that it is possible to reduce the manufacturing cost through the experience of full-scale structure manufacturing for Automated Fiber Placement (AFP) manufacturing, which is expected as a manufacturing method suitable for this design method. Regarding fiber orientation optimization, tow steering (curved tow) along the load flow using AFP improves strength and makes it possible to reduce weight. Regarding the optimization of sheet thickness distribution, in conventional manual layup, frequent use of part thickness variations leads to an increase in manufacturing costs (fabrication time), but by utilizing AFP, the fabrication time can be shortened and fine variations in part thickness can be provided. This makes it possible to reduce the weight of the structure.

The fuselage frame around the emergency escape door of single-aisle aircraft was selected as a part where cost reduction effect by AFP manufacturing and weight reduction by application of optimization design method are expected. We examined and applied the optimization design method to the target part and confirmed its effectiveness by comparing it with the conventional design method (Fig.5.2.1). A test concept for evaluating the effect of the optimization design method on the actual structure was studied, and the basic design of the test article and the layup mandrel necessary for the fabrication of the test article was carried out. A test article was manufactured, and the test was conducted in January 2023.

5.3 Clarifying Edge Glow Mechanisms of CFRP Exposed to Simulated Lightning Current in In-plane Direction

Shintaro Kamiyama¹, Takao Okada¹, Hiromitsu Miyaki¹, Yoshiyasu Hirano¹, Takeo Sonehara², Toshio Ogasawara³

¹ Japan Aerospace Exploration Agency, Tokyo, Japan

² Shoden Corporation, Tokyo, Japan

³ Tokyo University of Agriculture and Technology, Tokyo, Japan

Carbon fiber reinforced plastics (CFRP) have been widely applied to primary structures of aircraft because of its high specific strength and stiffness. One of the serious hazards for aircraft structures made by CFRP is lightning during operation [1]. Edge glow is visible light at cut edge of CFRP structure due to lightning current passing through composite materials [2]. Edge glow might be ignition risk when it occurs in the fuel tank made of composite material, therefore, it must be understood and mitigated to ensure the safety of aircraft. However, fundamental nature of the phenomena has not been generally understood. Especially, fundamental generation process of edge glow is not understood in detail because edge glow was evaluated by using still camera images in many earlier works. Objective of this study is to clarify the mechanisms of edge glow of CFRP exposed to lightning current. To achieve this objective, simulated lightning current was directly applied to rectangular shape CFRP laminates specimen. Phenomena was observed by using a high-speed camera. Numerical analysis based on finite element analysis (FEA) was also carried out to estimate Joule heating generation and voltage distribution.

CFRP laminates were fabricated by using unidirectional carbon fiber/toughened epoxy prepreg tapes (IMS60/#133, Teijin, Japan). Stacking sequence of two kinds were prepared; CP [0/90]_{4s}, and QI [45/0/-45/90]_{2s}. Each specimen had 50 mm width, 150 mm length and 2.3 mm thickness. Each specimen was set between two copper plate electrodes as shown Fig. 5.3.1. To reduce contact resistance between copper plate electrodes and specimen, copper was plated on the short edge of specimen. One copper plate electrode was connected to an impulse current generator (Haefely Hipotronics), which applied modified component A waveform in accordance with SAE ARP 5412B, while another electrode was connected to ground. Maximum

current was set to 10 kA, and T_1/T_2 was 13/70 μ s. Phenomena during application of lightning current were observed by using a high-speed camera at 500 kfps.

Numerical analysis based on finite element analysis (FEA), which was reported in our earlier works in detail [3], were carried out to calculate voltage and temperature distribution. Numerical analysis model was shown in Fig. 5.3.2. To reduce numerical cost, half model was built up. For electrical boundary conditions, surface current, which was calculated by lightning current obtained from experiment divided by electrode area, was applied to one electrode and the other electrode was set to electrical ground. Contact resistance between electrode and specimen was not considered to simplify phenomena. For thermal boundary conditions, thermal radiation was considered. The emissivity of surface was set to 0.9, and initial temperature of specimen and copper plate electrode were defined as 22°C.

Fig. 5.3.3 shows high-speed camera images of CP and QI laminate when 10 kA of lightning current was applied. While nothing was observed in the CP laminate, edge glow was detected on long edge of specimen in the QI laminate. High-speed images revealed that edge glow started at 4 μ s after application of impulse current in QI laminate. Fig. 5.3.4 shows the temperature distribution on long edge of QI laminate obtained by FEA when 4 μ s after application of impulse current. The image was magnified by 30 times in thickness direction for easy evaluation. Temperature of 0° layer was increased to approximately 24°C. Fig. 5.3.5 shows electrical field norm distribution, which indicates voltage gradient, 4 μ s after application of impulse current. Electrical potential of CP laminate was distributed uniformly in thickness direction. On the other hand, that of QI laminate was distributed ununiformly in thickness direction because of the effect of 45° layer. Therefore, the order of electrical field norm of QI laminate was 1000 times larger than that of CP laminate. Moreover, it is generally known dielectric strength of air is 3 kV/mm, which is close to numerically obtained result. Therefore, these experimental and numerical results indicate that occurrence criteria of edge glow are not increasing temperature but increasing electrical field (electrical voltage gap between layers).

References

- [1] L. Chemartin et al., J Aerosp Lab pp. 1-15 (2012).
- [2] R.B. Gregor et al., ICOLSE15 proceeding (2015).
- [3] S. Kamiyama et al., Compos Part A Appl Sci Manuf, 107111 (2022).

Acknowledgement

This work was supported by JSPS KAKENHI, Grant Numbers 22K14427 and 22H01691. We would like to give special thanks to Mr. Katsunori Takida and Mr. Kouichi Asaka of IHI Jet Service Co., Ltd., for their technical support.

5.4 Aircraft Accident and Serious Incident Investigation Yasuhiro Yamada

Japan Transport Safety Board (JTSB), Tokyo, Japan

(1) Total number of registered aircraft in Japan

As of December 31, 2021, the number of registered civil aircraft in Japan was 2,843, consisting of 1,342 airplanes (of which 652 airplanes are equipped with jet engines), 851 helicopters, 649 gliders inclusive of motor gliders, and one airship.

(2) Statistics related to the accident and serious incidents investigation

The number of accidents and serious incidents which JTSB investigated in the past two years are shown in Tables 5.4.1 and 5.4.2 of a total of 57 occurrences, large airplanes accidents and serious incidents were 12, small airplanes were 17 and rotorcraft were 13. Gliders, ULPs (ultra-light planes) and others were remaining 15 occurrences.

(3) Fatigue failure related serious incident

1) Summary of the serious incident

While a Boeing 777-200, registered JA8978 and operated by Japan Airlines Co., Ltd. As its scheduled flight 904, was climbing after take-off from Naha Airport for Tokyo International Airport on December 4, 2020, there occurred an abnormal sound accompanied by shaking of the aircraft, and the instrument displayed anomaly in the left engine (No. 1 engine) at an altitude of FL170 over the sea approximately 50 km north of Naha Airport. The captain shut down the engine and landed back at the airport after declaring a

state of emergency to the air traffic controller. In the post-flight inspection, it was confirmed that two fan blades of the left engine were fractured, the fan cowl door and other fragments from the nacelle had separated and departed the airplane, and the fuselage and horizontal stabilizer were damaged from impact of fragments. There were 189 people onboard, consisting of the captain, 10 crew members, and 178 passengers. There were no injuries.

2) Detail of the Damage

Among the 22 Fan Blades on the Left Engine, Fan Blade No.16 fractured in the flow path and Fan Blade No.15 fractured in the mid-span area, and all of the fragments of these blades were not found (Figure 5.4.1). Fatigue fracture was observed in the fractured surface of Fan Blade No. 16.

3) Detailed investigation of Fan Blade No. 16

The hollow part located in the fan blade is called “cavity” that is divided into 7 areas to which AA through GA are assigned from the LE side (Figure 5.4.2). Detailed visual investigation of the fillet on the fracture surface of the convex side of the cavity FA of the Fan Blade revealed beach marks and radial marks that were characteristic of fatigue fracture. Cracks were radially progressed from the origin to the convex side of the Fan Blade (Figure 5.4.3).

A nodule was located at the fatigue origin. FESEM (Field Emission Scanning Electron Microscope) examination of the nodule revealed the composition of the nodule was predominantly titanium with some aluminum and oxygen, which was similar to the Fan Blade material (Ti-6Al-4V) (Figure 5.4.3).

The engine manufacturer had already grasped the condition of the nodules like this, judged that this was caused by polishing performed in the condition of an insufficient cooling and machining process of manufacturing fan blades, which led to “Spark Impingement” where a molten metal scattered as a spark and collided with and deposited to the base material while heated.

To identify the time when fatigue fracture occurred, based on a striation count, crack growth assessment was conducted. From the number of the striation, the fatigue crack was estimated to initiate over 6,000FC ago, and approximately 0.055-inch-deep when inspected in the last TAI (Thermal Acoustic Image) inspection (3,633 FC prior) conducted in June 2018. However, most likely this was not detected at that time.

4) Defect Detection Capability of TAI Inspection

The defect detection at the part of the fillet by TAI inspection was most likely difficult since the POD (Probability of Detection) of the crack depth was approximately 35% as seen from Flow path CV-Fillet (dark blue color) in Figure 5.4.4.

Plate thickness of each zone of the Fan Blade became thicker from the mid span area through the root section, and the fillet was thicker than the flat region. From the nature of TAI inspection that utilizes the method to detect the thermal response of defects by the temperature rise of the blade surface, the thicker a plate becomes, the more the defect detection accuracy deteriorates.

TAI inspection intervals for fan blades were set by the engine manufacturer to secure 90% or more of POD. The JTTSB concludes, however, that TAI inspection intervals were set based on POD evaluation conducted on flat regions without thorough consideration of TAI inspection characteristics that detection accuracy of defects in fillet regions deteriorates because there have been no cases where defects occurred in the fillet up till then.

5) Analysis of Findings

The JTTSB concludes that this was a serious incident certainly caused by the fan blades of the left engine were fractured during take-off climb, resulting in parts and cowlings of the engine were departed, and the airframe was damaged by scattered parts.

The JTTSB concludes that it is highly probable that the fracture of the fan blade had initiated from the nodule, which bonded to the internal surface of a hollow structure during the polishing process of manufacturing of the fan blades, and the crack was generated, in addition to this, the aircraft continued flights without detecting the crack at the subsequent regular inspections led to fatigue fracture.

The JTTSB concludes that it is probable that the cracks were not detected in the subsequent regular inspections were contributed by method and intervals of the used inspection were insufficient to detect the defect in the fillet region.

ACKNOWLEDGEMENT

The editor appreciated the members of the ICAF national committee of Japan Society for Aeronautical and Space Sciences and other participants in the committee, for their contribution in preparation of this national review and contributing discussion in the committee.

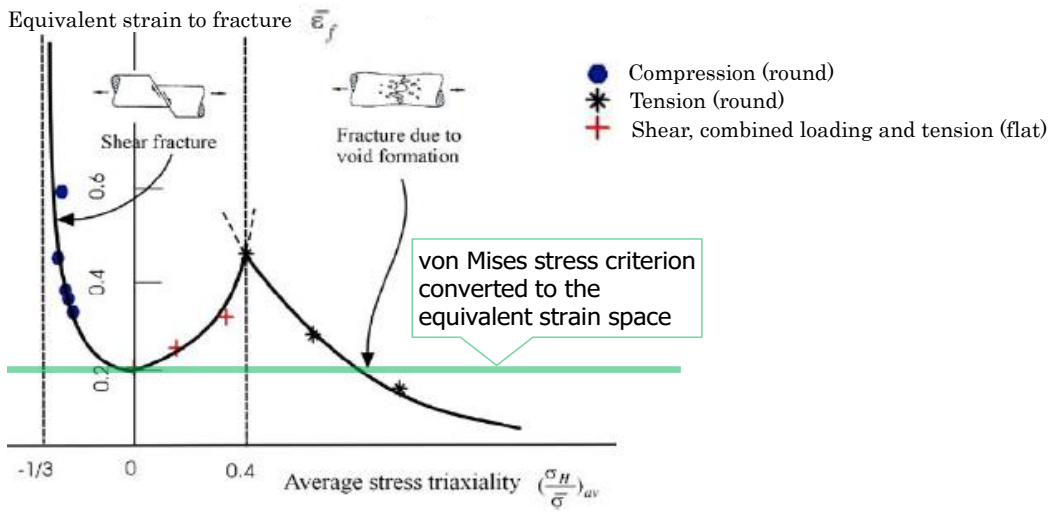


Figure 2.1.1 Ductile fracture behavior under various stress states [1].

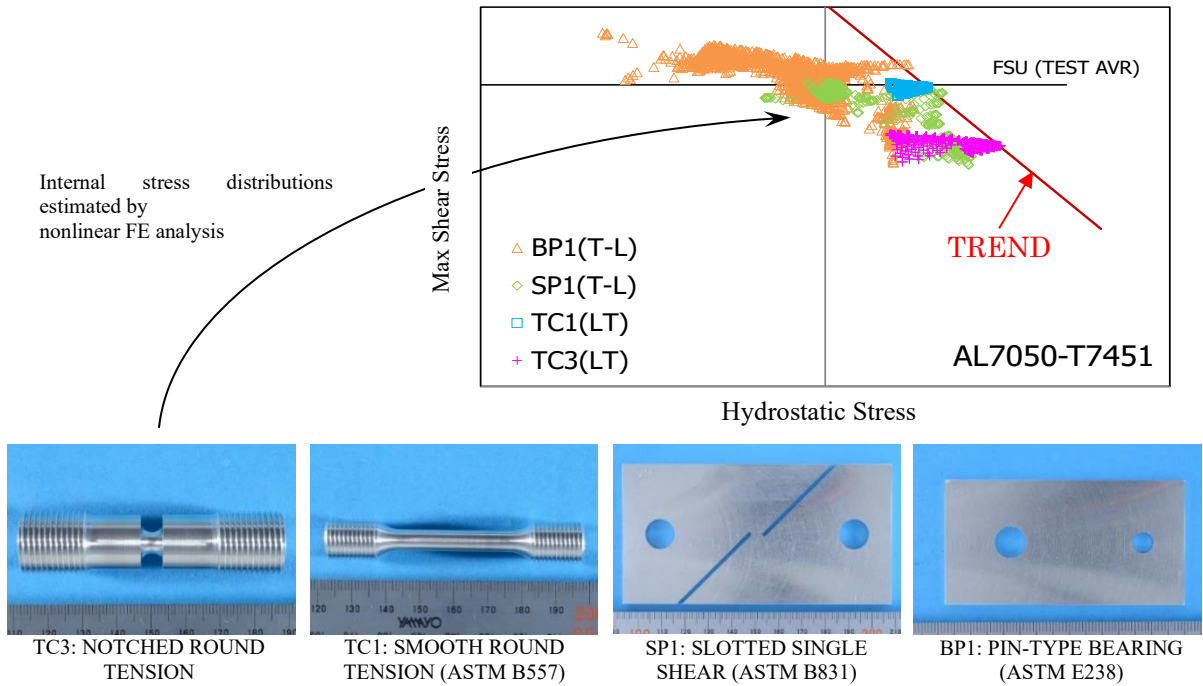


Figure 2.1.2 Estimated internal stress state at the instance of specimen fractures

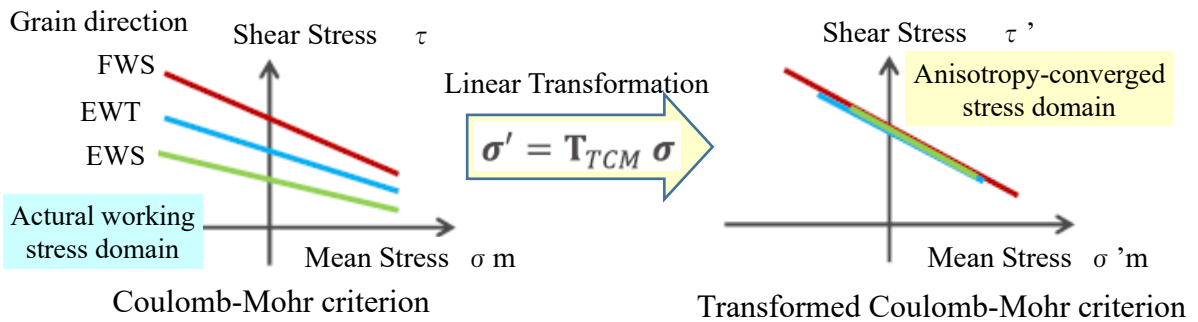


Figure 2.1.3: Transformed Coulomb-Mohr Model

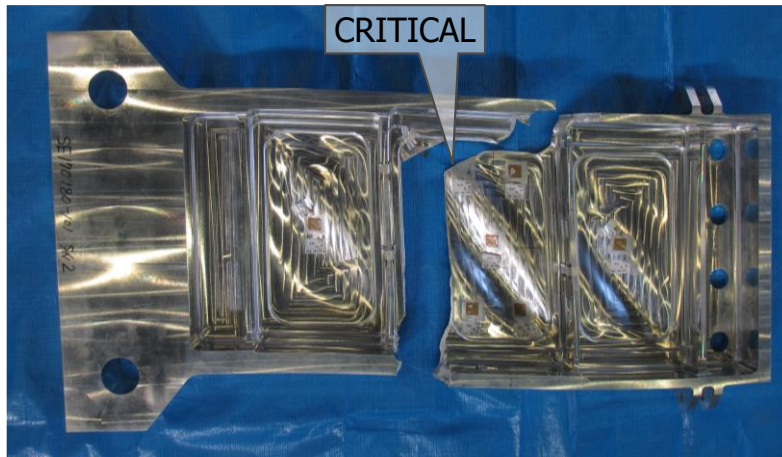


Figure 2.1.4 Fractured test specimen

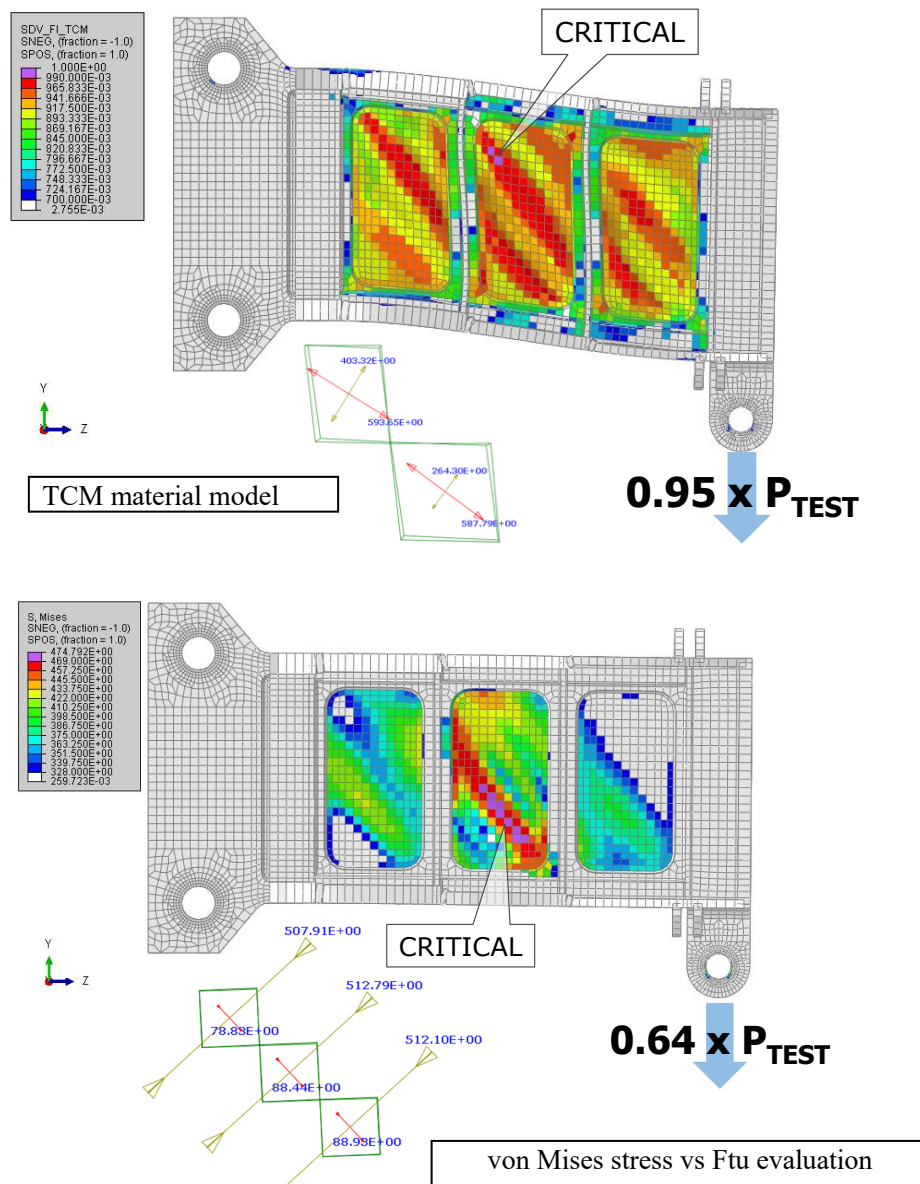
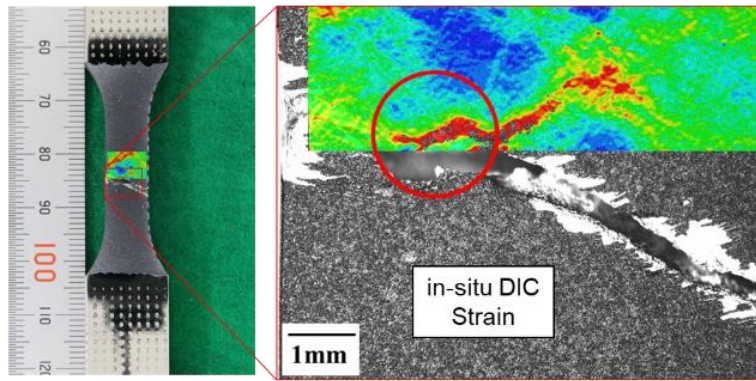


Figure 2.1.5 Ductile fracture predictions

In-situ DIC dwell fatigue testing



Fractography to detect origin

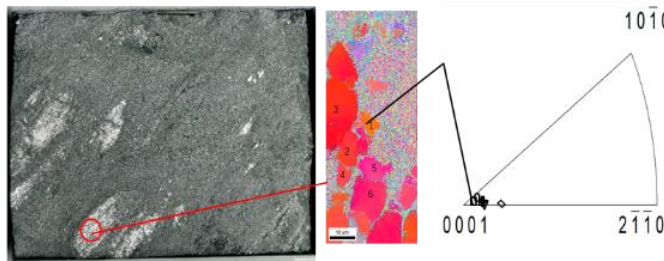


Figure 2.2.1 In-situ DIC Dwell fatigue testing and quantitative fractography

Crystal Plasticity FEM model*

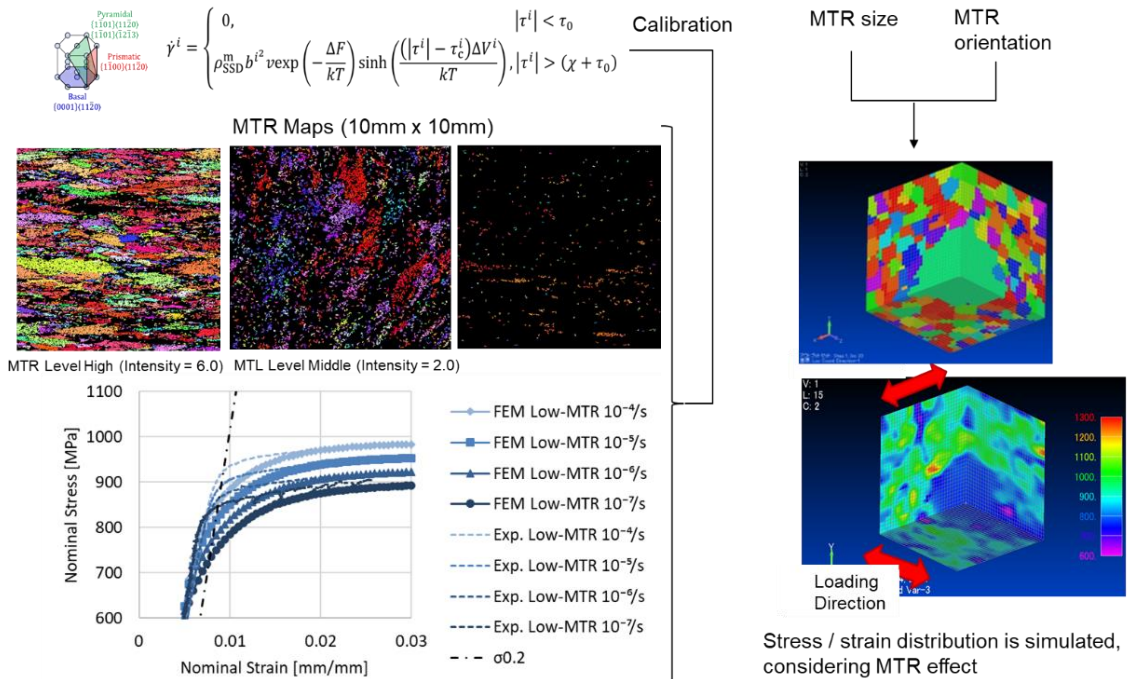


Figure 2.2.2 Crystal plasticity FEM model to predict dwell fatigue life reduction

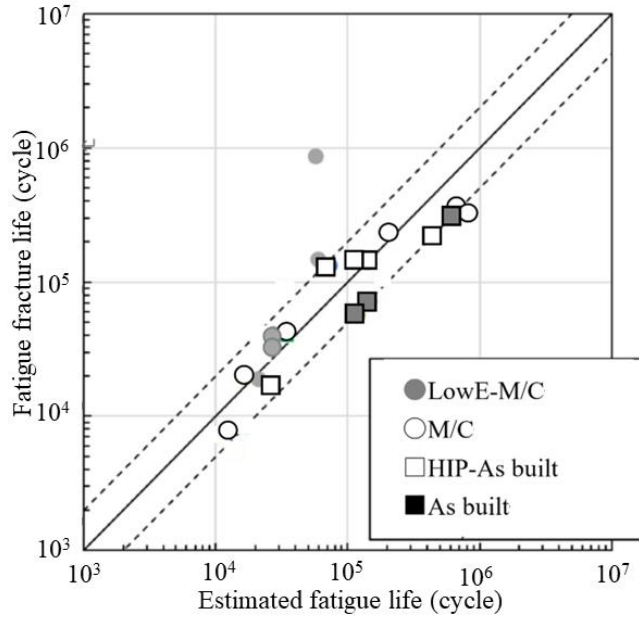


Figure 2.3.1 Comparison of estimation result and fatigue test result

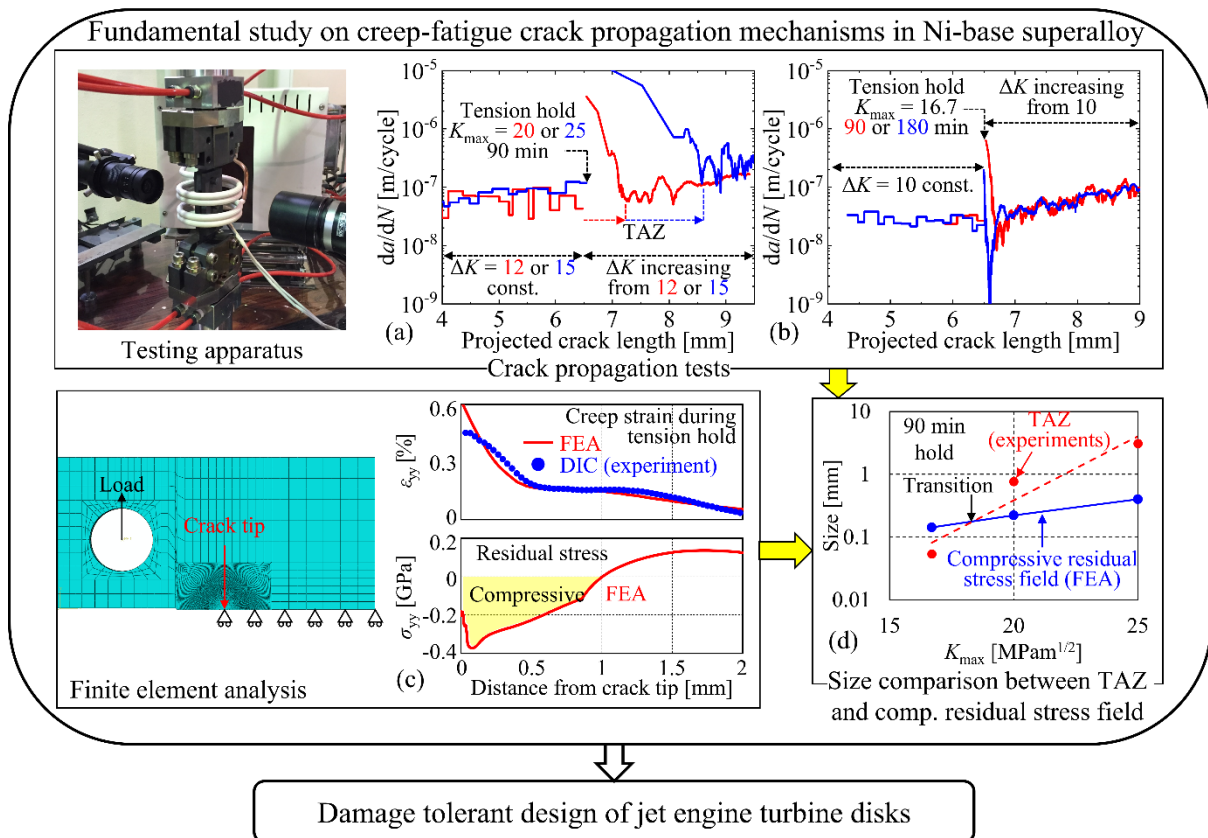


Figure 2.4.1 The schematic of this study

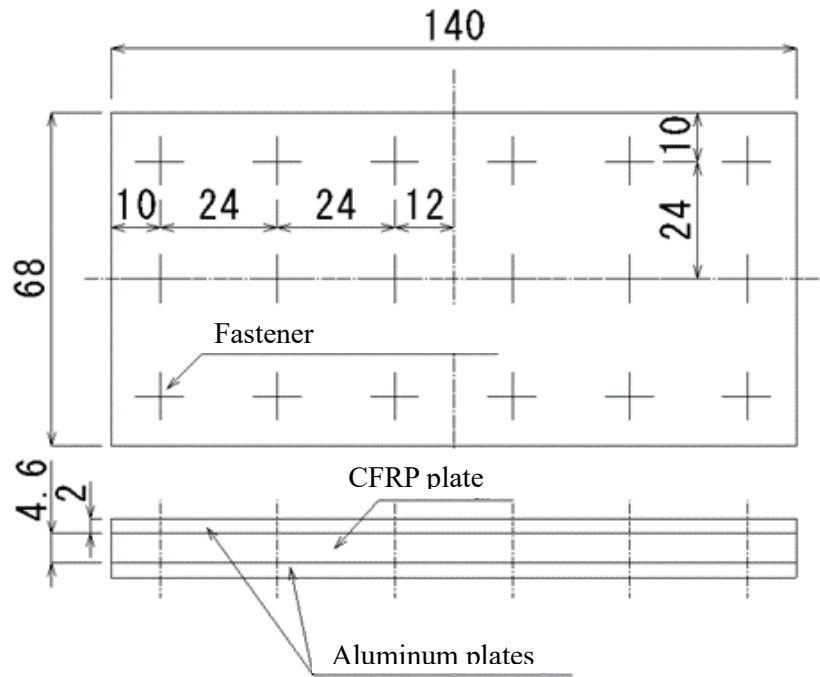


Figure 2.5.1 CFRP/Aluminium alloy hybrid joint specimen

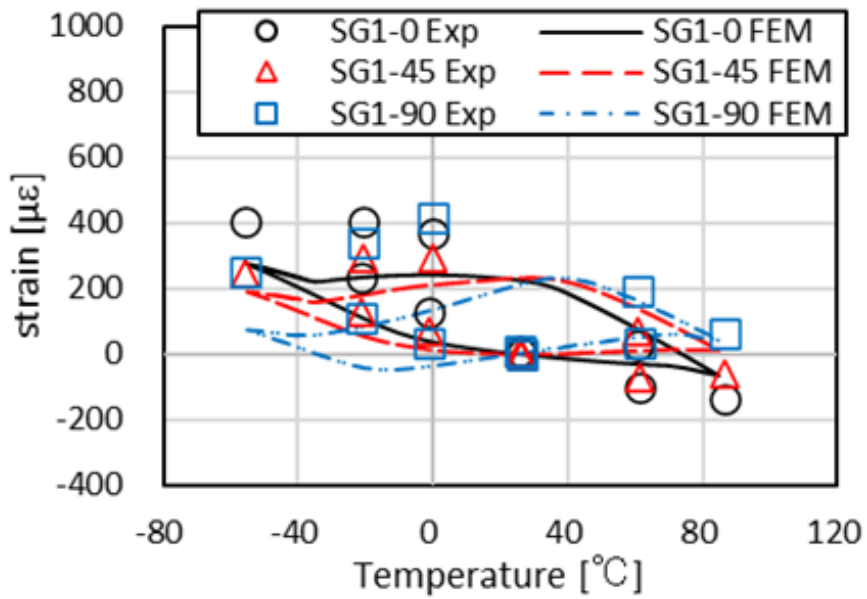


Figure 2.5.2 Hysteresis of elastic strain against temperature at gauge 1

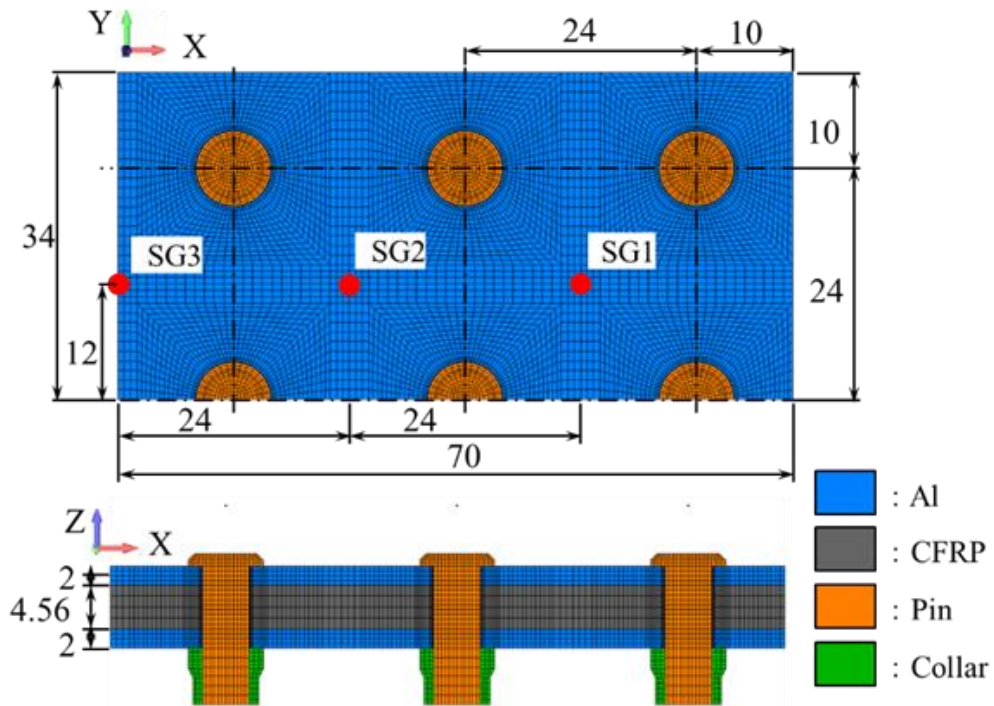


Figure 2.5.3 FEM model of the CFRP/Aluminium hybrid joint

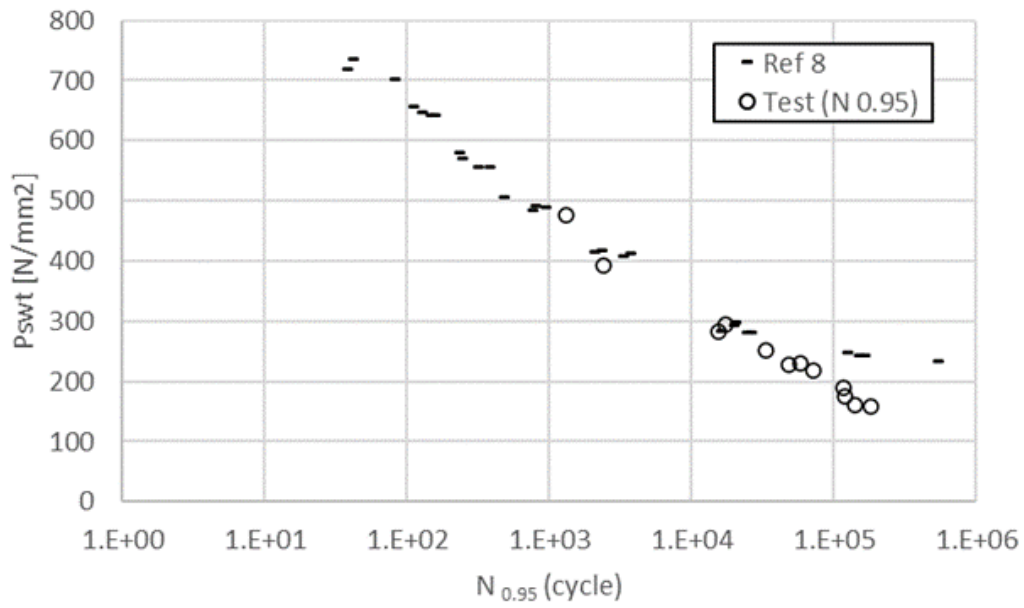


Figure 2.5.4 Relationship between product of maximum stress by strain amplitude and fatigue cycles

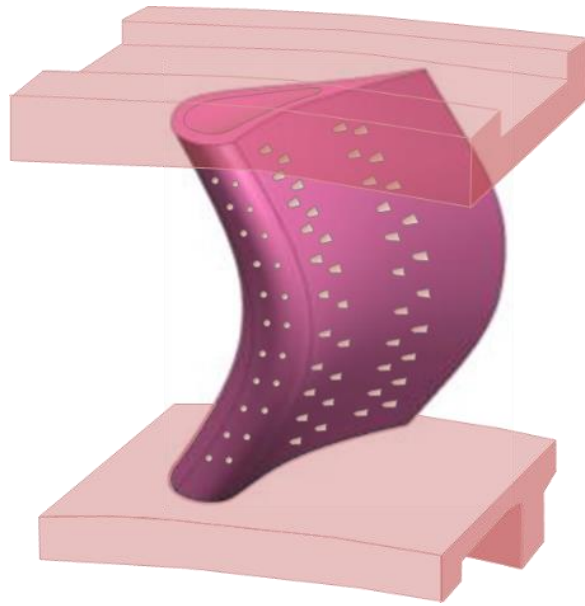


Figure 3.1.1 Next generation turbine vane concept proposed in En-Core project.

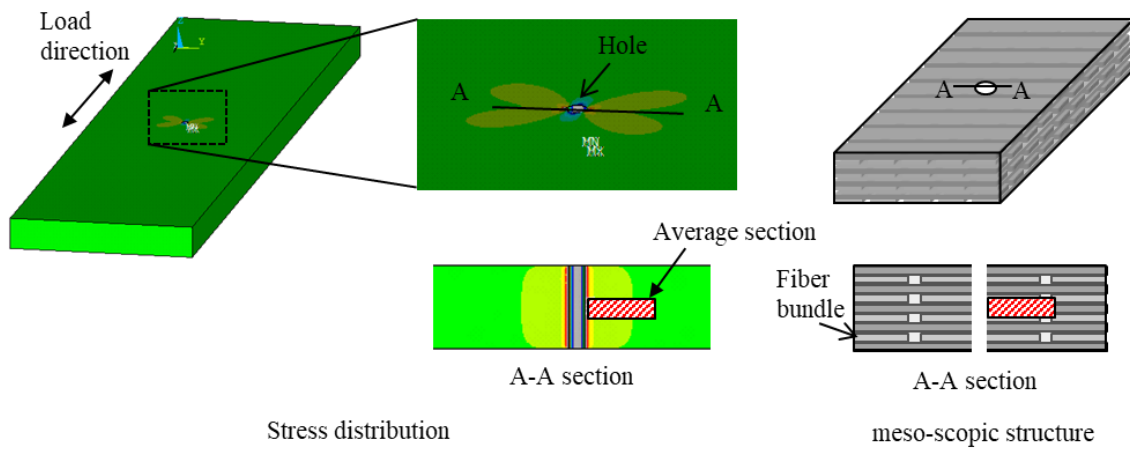


Figure 3.1.2 Section size and direction on the calculation for evaluation stress

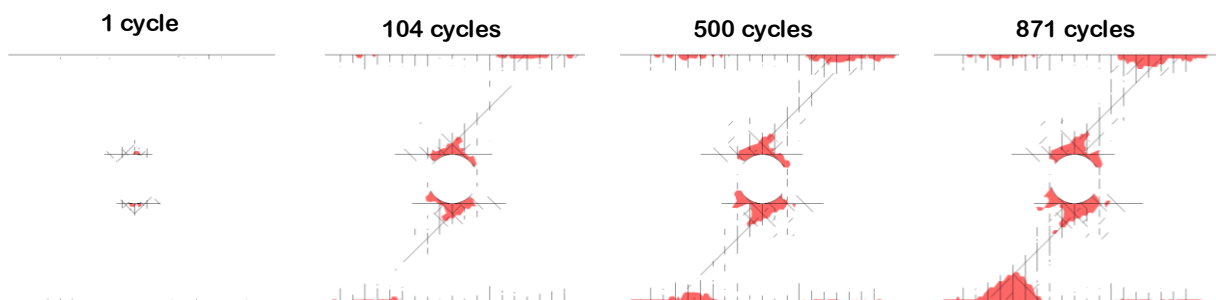


Figure 3.2.1 Damage progress predicted by CZM-XFEM

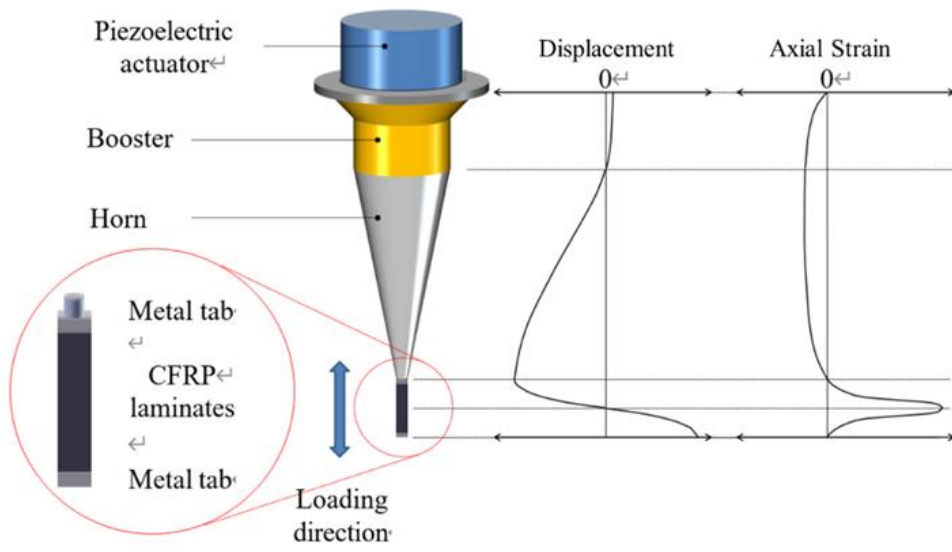


Figure 3.3.1 Schematic of ultrasonic fatigue testing for CFRP laminates

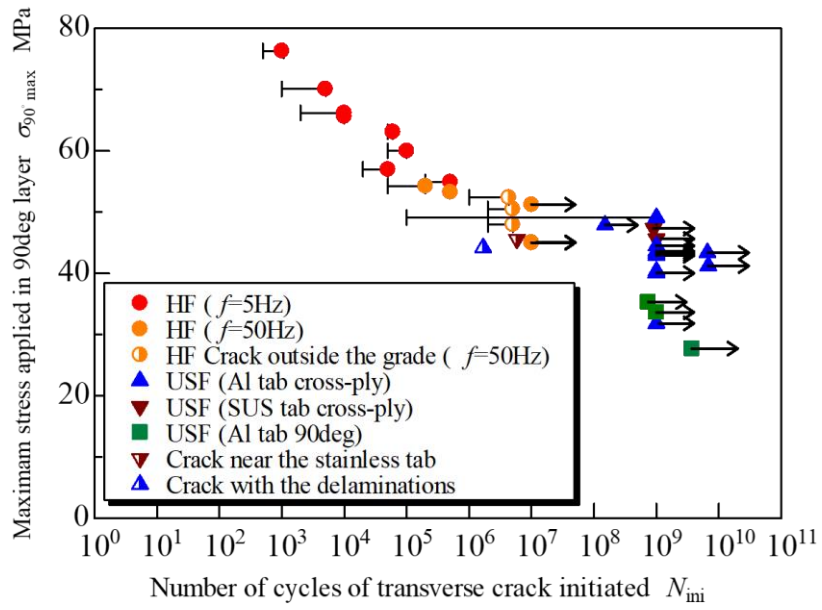


Figure 3.3.2 S-N diagram for transverse crack initiation in cross-ply CFRP laminates.

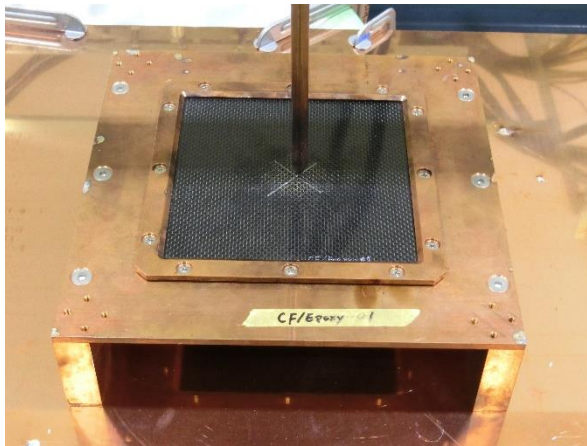


Figure 3.4.1 Setup of the lightning test specimen

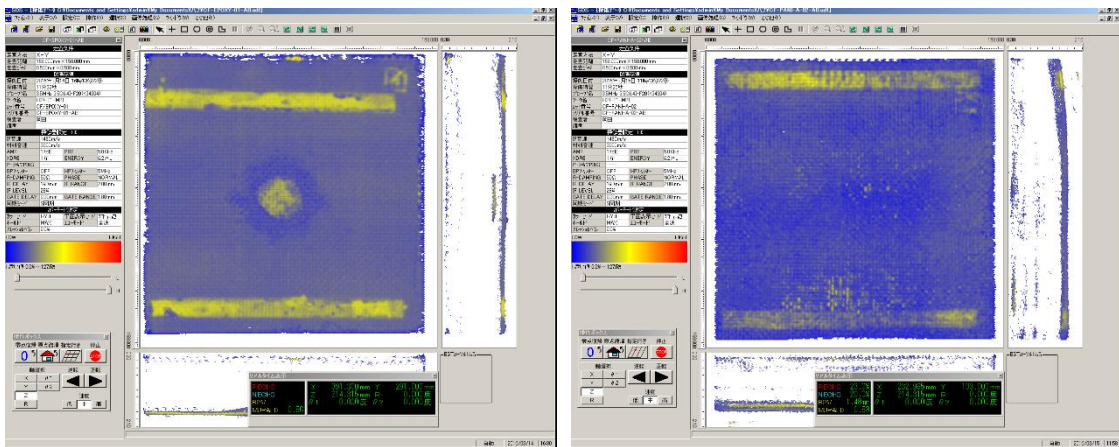


Figure 3.4.2 NDI results for CFRP specimens (left: conventional, right: electrically conductive)

Table 3.5.1 Comparison required times between conventional visual procedure and automated procedure with crackgage (Unit: min.)

Procedure	Setting crackgage on specimen (Adhesive)	Connecting crackgage to device and setting strain amplifiers	Operator restraint time in carried out test	Total time
Conventional visual	0	0	240	240
Automated with crackgage	40	15	5	60

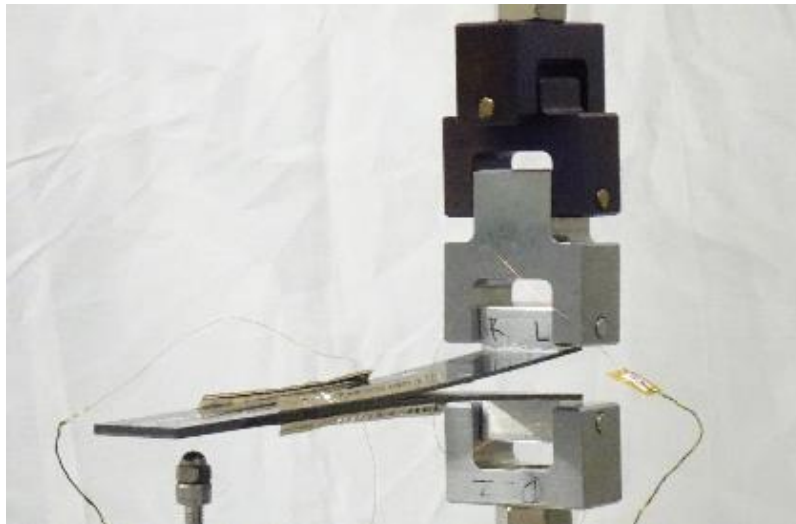


Figure 3.5.1 DCB test specimen and test fixture with 70 mm crack gages.

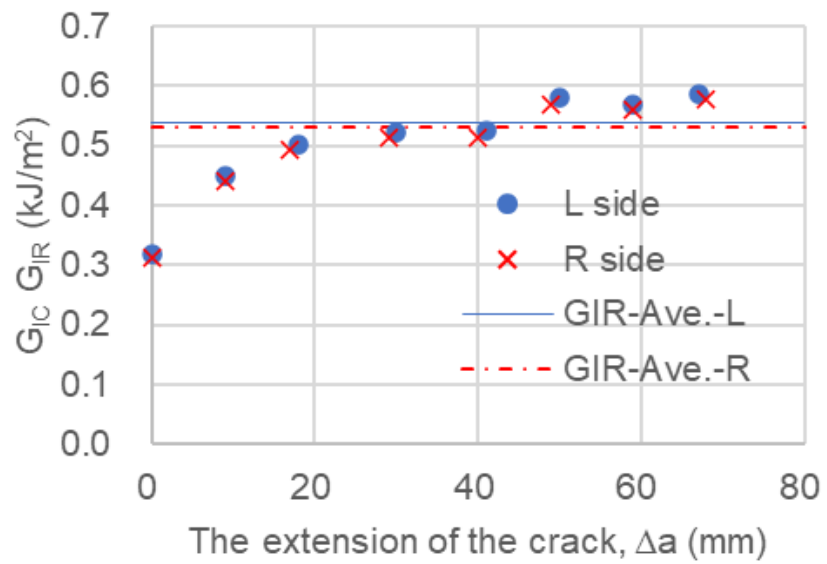


Figure 3.5.2 R-Curve from DCB test

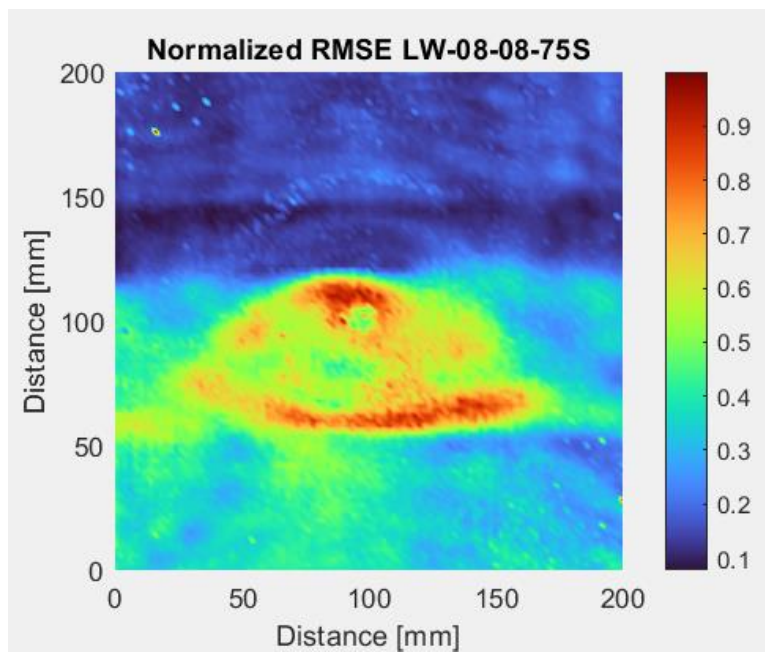
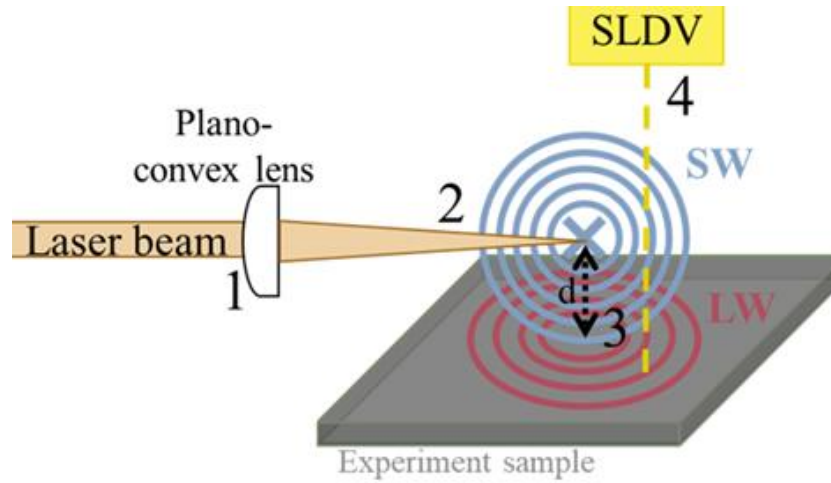


Figure 4.1.1 Schimatic image of damage detection by Lamb wave and example of obtained results

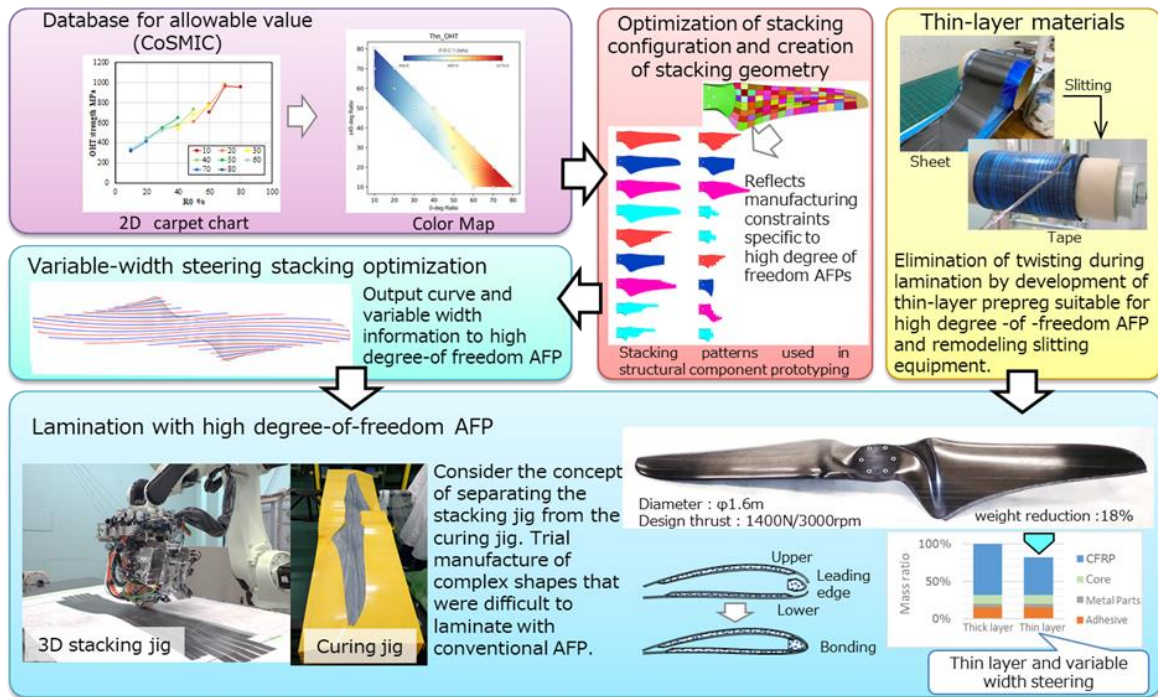
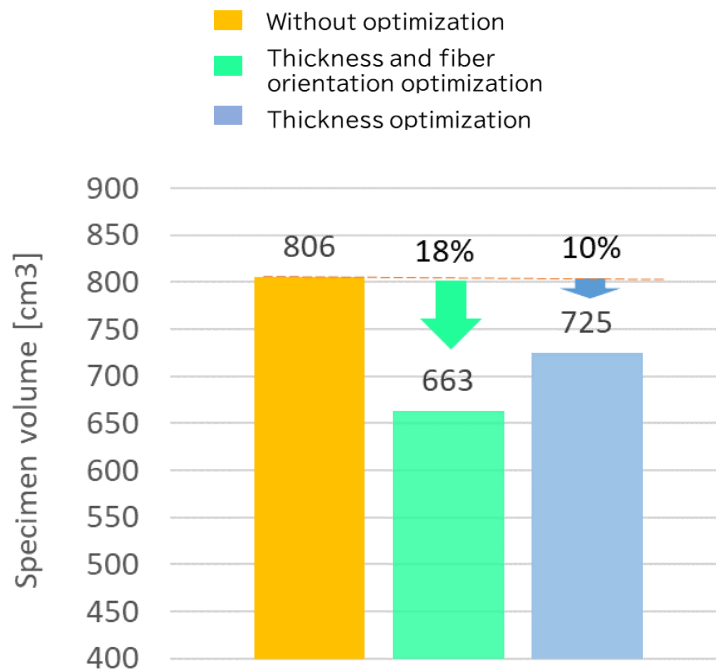


Figure 5.1.1 The schematic of this study



Weight reduction effect by adaptive design

Figure 5.2.1 Weight reduction by adaptive design

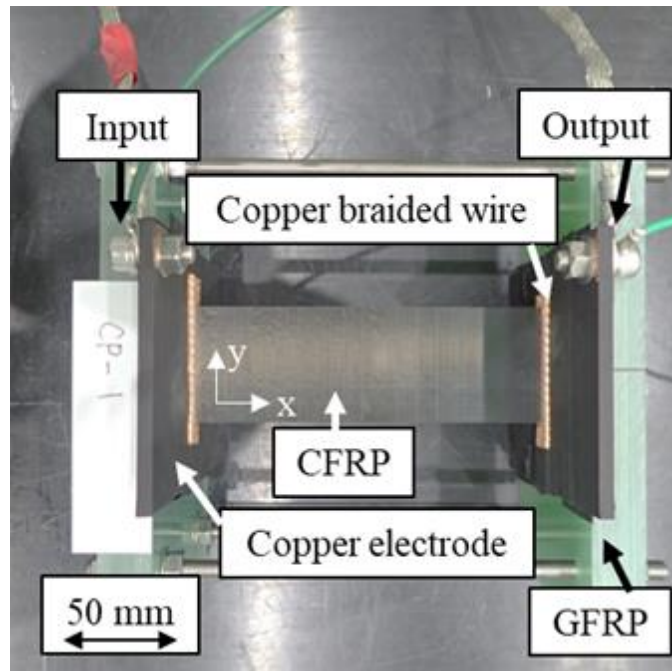


Figure 5.3.1 Experimental setup.

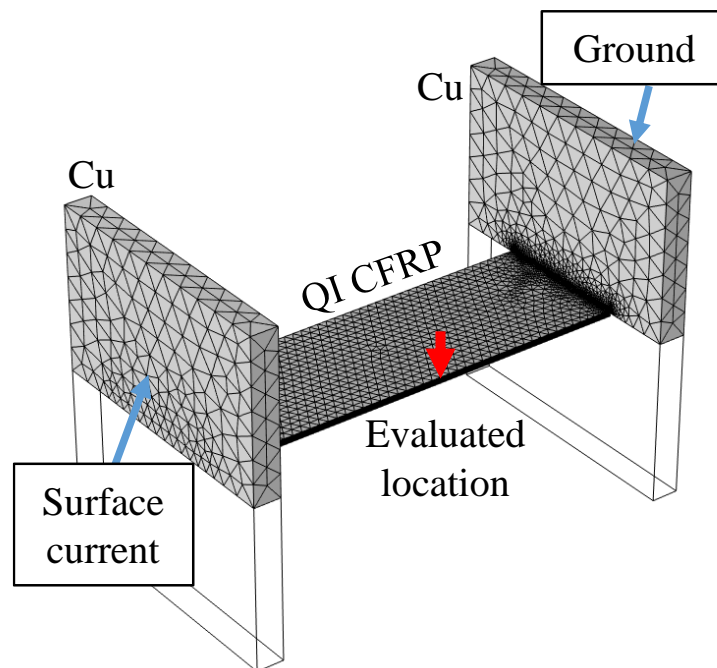


Figure 5.3.2 FEA model and boundary conditions.

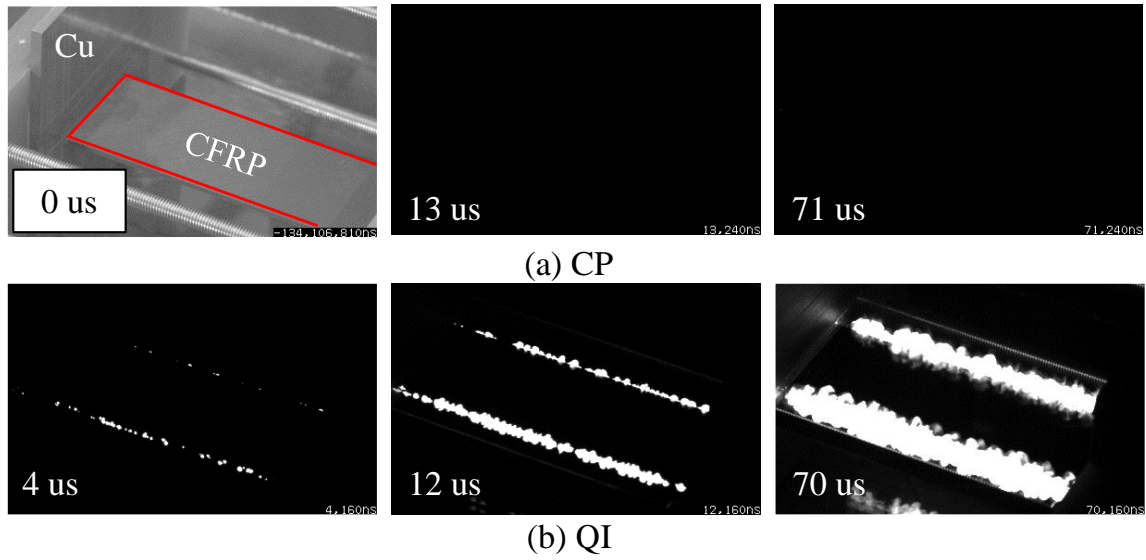


Figure 5.3.3 High-speed images when 10 kA of lightning current was applied.

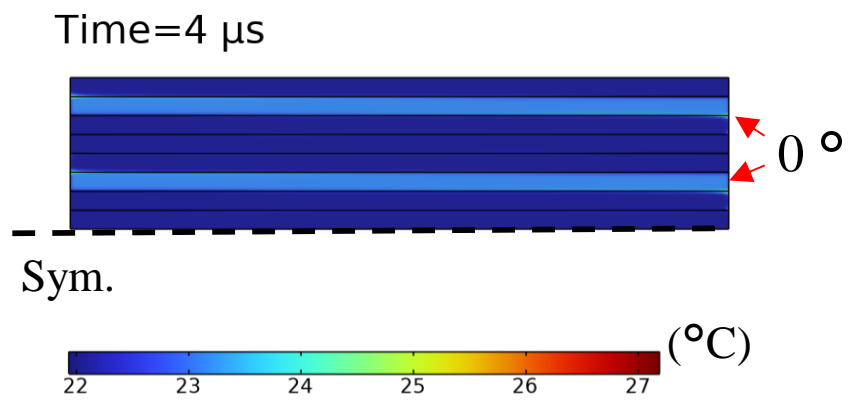


Figure 5.3.4 Temperature distribution of QI laminate.

Time=4 μ s



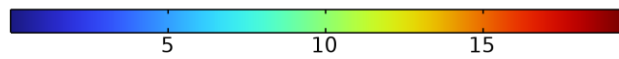
(V/mm)



(a) CP



(kV/mm)



(b) QI

Figure 5.3.5 Electrical field norm distribution.

Table 5.4.1 Number of Accident by Type of Aircraft

Aircraft Year	Large Airplane	Small Airplane	Rotorcraft	Glider, ULP or others	Total
2021	1	2	3	5	11
2022	8	4	3	6	21

Table 5.4.2 Number of Serious Incident by Type of Aircraft

Aircraft Year	Large Airplane	Small Airplane	Rotorcraft	Glider, ULP or others	Total
2021	1	4	3	2	10
2022	2	7	4	2	15



Figure 5.4.1 Fractured Fan blades

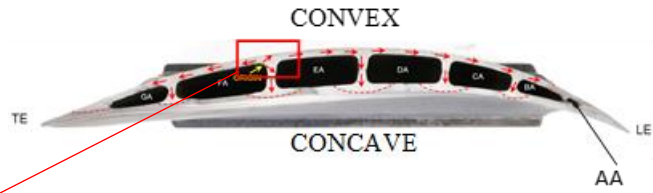


Figure 5.4.2 Fractured surface No.16 Fan blade

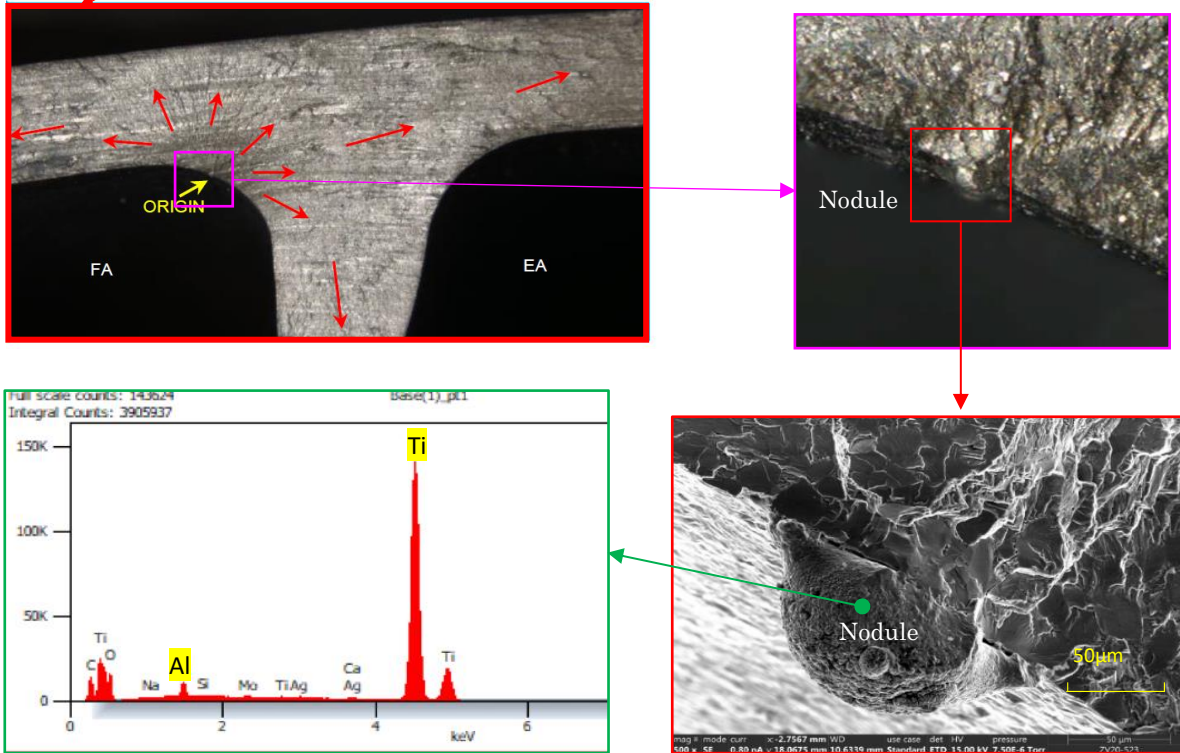


Figure 5.4.3 Origin of the fatigue fracture and Composition of the nodule

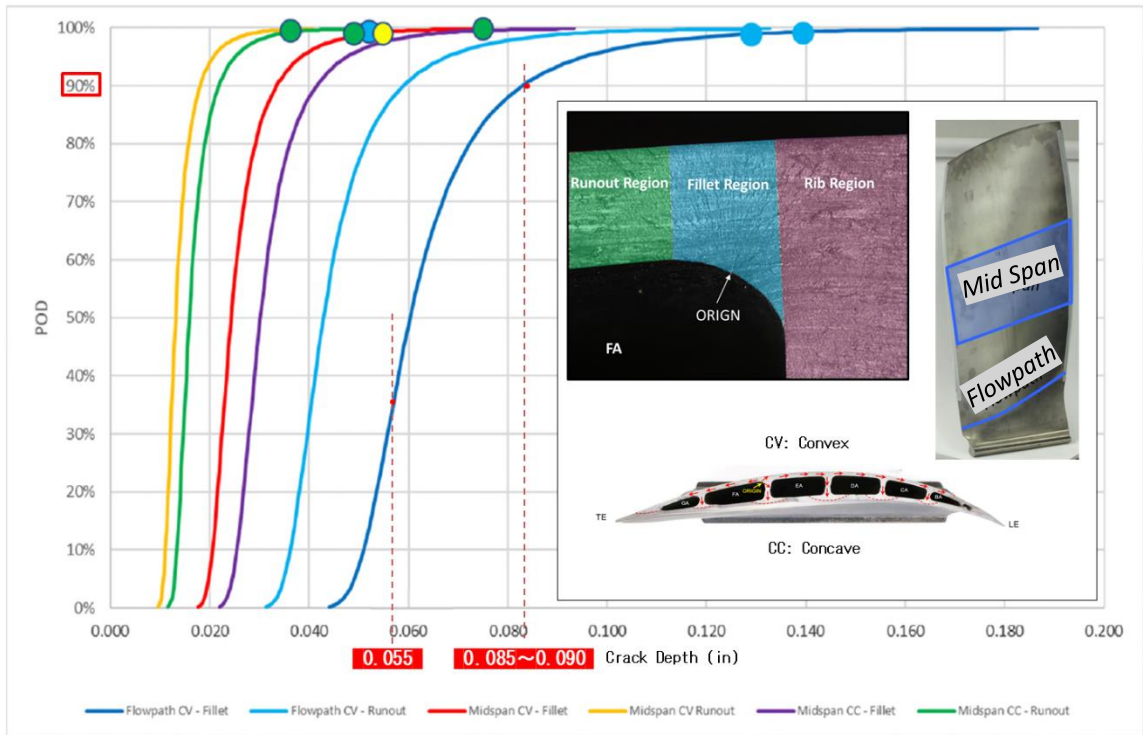


Figure 5.4.4 TAI POD CURVES